Activation of Somatostatin Inhibitory Neurons by Lypd6-nAChRα2 System Restores Juvenile-like Plasticity in Adult Visual Cortex

Masato Sadahiro[1-5]†, Michael P. Demars[1-5]†, Poromendro Burman[1-5], Priscilla Yevoo[1-5], Milo R. Smith[1-5], Andreas Zimmer[6], Hirofumi Morishita[1-5]*

[1] Department of Psychiatry, [2] Department of Neuroscience, [3] Department of Ophthalmology, [4] Mindich Child Health and Development Institute,[5] Friedman Brain Institute, Icahn School of Medicine at Mount Sinai, 1 Gustave L. Levy Pl, New York, NY 10029, USA

[6] Institute of Molecular Psychiatry, Medical Faculty, University of Bonn, Bonn 53127, Germany

*Contact to: hirofumi.morishita@mssm.edu

† M.S. and M.P.D. share co-first authorship

Abstract

Heightened juvenile cortical plasticity declines into adulthood, posing a challenge for functional recovery following brain injury or disease. A network of inhibition is critical for regulating plasticity in adulthood, yet contributions of interneuron types other than parvalbumin (PV) interneurons have been underexplored. Here we show Lypd6, an endogenous positive modulator of nicotinic acetylcholine receptors (nAChRs), as a specific molecular target in somatostatin (SST) interneurons for reactivating cortical plasticity in adulthood. Selective overexpression of Lypd6 in adult SST interneurons reactivates plasticity through the α2 subtype of nAChR by rapidly activating SST interneurons and in turn inhibiting sub-population of PV interneurons, a key early trigger of the juvenile form of plasticity. Chemogenetic activation of SST interneurons confirms the causal role of SST interneuron activity in reactivating plasticity. Collectively, we identify the Lypd6-nAChRα2 system and associated SST-PV disinhibitory microcircuit as the novel SST interneuron-specific targets for reactivating plasticity in adulthood. This provides potential insights into therapeutic strategies against disorders where recovery is limited due to diminished plasticity in adulthood, such as amblyopia and psychiatric disorders characterized by deficits in SST interneurons.

(178 words)

Introduction

Experience-dependent brain plasticity is heightened during juvenile critical periods but this declines into adulthood, which poses a major challenge to functional recovery following injury or disease later in life [1,2]. A prevailing concept of therapeutic strategy to support restoration of function from such enduring debilitating conditions is to reactivate juvenile-like levels of heightened plasticity in the adult brain. One of the best-studied models of critical period plasticity is ocular dominance plasticity – the enduring loss of responsiveness in primary visual cortex (V1) to an eye deprived of vision [3] that results in amblyopia, a disorder of sight with limited treatment options in adulthood that affects 2–4% of the human population. The ocular dominance plasticity model has long served to not only to advance our understanding of the fundamental regulatory mechanisms of critical periods, but also importantly to facilitate the discovery of novel targets to achieve reactivation of visual plasticity in adulthood.

Over the past decade, with the advent of gene targeting in mice [4-7], the network of cortical inhibition was elucidated as one of the critical mechanisms for regulation of visual plasticity. The developmental initiation of the critical period can be accelerated or delayed by genetically or pharmacologically altering GABAergic inhibition in visual cortex [8-16]. Following critical period closure in the adult cortex, plasticity can be induced through pharmacological suppression of $GABA_A$ receptors [17] or through the transplantation of GABAergic precursors derived from the medial ganglionic eminence (MGE) [18-20]. To date, the role of GABAergic signaling in cortical plasticity has largely focused on parvalbumin (PV) interneurons [15,18,21-23], where a number of known molecular mediators of plasticity appear to converge including orthodenticle homeobox protein 2 (otx2) [15,24] and perineuronal nets [23]. A recent report has shown that PV interneuron activity is reduced during the initial 24 hours following visual deprivation only during the juvenile critical period but not in adulthood. Mimicking this early reduction in firing using chemogenetic means in adult animals led to reactivation of plasticity, suggesting that PV interneuron activity may be instructive for plasticity in visual cortex [22]. While their importance for plasticity in the visual cortex is undeniable, PV interneurons represent only one member

of a diverse group of cortical GABAergic interneurons [25]. The role of other major subclasses of GABAergic interneurons, such as those expressing the peptide somatostatin (SST) that represent nearly a third of the cortical GABAergic interneurons, had largely been unquestioned until recently [19,26]. Moreover, the existence of molecular and circuit mechanisms underlying SST interneuron-mediated regulation of cortical plasticity remains completely unknown.

SST interneurons are promising targets for reactivating plasticity in the adult brain, as they are ideally situated to integrate multiple inputs including bottom-up sensory signals [27], or neuromodulation [28] induced by locomotion [29-33] or by top-down regulation [34-36]. Moreover, SST interneurons robustly innervate local PV interneurons, which places them in an ideal position for driving the rapid inhibition of PV interneurons that is causal to the juvenile form of plasticity. Neuromodulation of SST interneurons, by nicotinic signaling that occurs in several brain regions [28,37-39], may represent one potential means of restoring plasticity in the adult brain. Our previous study showed that an endogenous inhibitor of nicotinic Acetylcholine Receptors (nAChRs) known as Lynx1 is enriched in PV interneurons and actively limits plasticity in V1 following the critical period [40]. The Lynx family of proteins are GPI-anchored membrane proteins and a have unique toxin-like protein structure, which enables them to bind to the extracellular face of nAChRs expressed in the same cells and regulate their signaling [41]. Our recent study further showed that another closely related member of the Lynx family known as Lypd6 is enriched in V1 SST interneurons in [42]. Interestingly, in direct contrast to the action of Lynx1, Lypd6 has been shown to potentiate calcium currents through nicotinic receptors [43,44]. Here we sought to elucidate the potential for nicotinic modulation by Lypd6 in SST interneurons as regulators of ocular dominance plasticity. This work provides the first molecular mechanism specifically associated with SST interneurons for reactivating plasticity in adult visual cortex.

Results

Neuronal overexpression of Lypd6 prolongs ocular dominance plasticity into adulthood

First, we compared the expression profiles of Lypd6 between adult V1, where plasticity is limited, versus that of juvenile critical period. We performed *in situ* hybridization to label Lypd6 mRNA in V1 of mice at P28 (critical period) and >P60 (adult). We found that Lypd6 expression is significantly lower in the adulthood compared to juvenile period, which inversely correlates with the extent of ocular dominance plasticity (Fig. 1a, 1b). While Lypd6 expression was even higher at P18 (pre-critical period) (p18: 244.91 +/-19.28 normalized to p60 data in Fig. 1a, $p<0.05$ vs P28 or adult), interpretation of Lypd6 contribution to nicotinic signaling during the pre-critical period is confounded by various additional developmental changes that could impact nicotinic signaling beyond Lypd6 (e.g. nAChRs, cholinergic projections) [45].

Based on this declined Lypd6 expression in adult V1, we tested if overexpression of Lypd6 in adulthood could prolong ocular dominance plasticity beyond the V1 critical period, by utilizing a transgenic mouse line with pan-neuronal overexpression of Lypd6 (Lypd6Tg)[43]. Following a 4-day short-term monocular deprivation of the contralateral eye (4d MD), ocular dominance plasticity was assessed in anesthetized mice using a 16-channel linear silicone probe[46] (Fig. 1c). Each recorded V1 neuron was assigned an ocular dominance (OD) score based on the relative balance of the neuron's visually evoked responses to the visual stimulus independently presented to the contralateral and ipsilateral eye. Adult Lypd6Tg mice that underwent 4d MD displayed an overall significant shift in eye preference of the V1 (OD shift), away from the deprived contralateral eye and towards the non-deprived ipsilateral eye compared to adult Lypd6Tg mice that did not undergo any visual deprivation (no MD) or adult wild type (WT) mice that typically display no significant levels of plasticity regardless of visual deprivation (Fig. 1d). Cumulative distributions of ocular dominance index scores (ODI: -1=most ipsilateral dominant, 0=equal/binocular, 1=most contralateral dominant) for each recorded neuron from each cohort show a significantly higher percentage of single neuronal responses that are relatively ipsilateral dominant in the Lypd6Tg 4d MD mice compared to control groups (Fig. 1e). Lastly, individual

animal level comparisons of contralateral bias index (CBI) scores – the relative strength to which the visually evoked activity of V1 neurons from the contralateral eye dominates over that from the ipsilateral eye, show a significant decrease only in the Lypd6Tg 4d MD mice (Fig 1f). Altogether the results suggest that Lypd6 is a novel positive regulator of ocular dominance plasticity.

Lypd6 expression specifically in SST interneurons reactivates ocular dominance plasticity in adult V1

While the aforementioned experiments outline the sufficiency of neuronal overexpression of Lypd6 for prolonging ocular dominance plasticity into adulthood, the transgenic line does not provide temporal, spatial, or cell type information regarding this effect. In order to address these questions, we developed a Cre-dependent AAV vector for overexpressing Lypd6 (AAV8-DIO-EGFP-2A-Lypd6: AAV-Lypd6) (Fig. 2a). Our previous study established that Lypd6 is most highly expressed in SST interneurons in V1 with lower expression in a subset of glutamatergic neurons [42]. Therefore, we characterized Lypd6 overexpression in V1 SST interneurons through viral injection of AAV-Lypd6 into adult SST-cre mice, and in V1 glutamatergic neurons through dual viral injection of AAV-Lypd6 and an AAV with a Cre expression vector driven by a CamKII promoter (AAV8-CamKIIa-mCherry-Cre: AAV-CamKII-cre) into adult WT mice as it was done in previous reports [29,47]. The viral injections were adjusted to target the deep cortical layers in the area where the endogenous expression of Lypd6 has been previously reported to be localized[42]. The two viral injection conditions resulted in GFP expression restricted to either SST or glutamatergic populations, but overall both conditions presented robustly increased expression of Lypd6 in V1 (Fig. 2b, c, d, and Supplementary Fig. 1).

Next, we assessed the ability of SST or glutamatergic overexpression of Lypd6 in V1 of adult animals to induce ocular dominance plasticity. We injected AAV-Lypd6 or control AAV vector (AAV8-hSyn-DIO-EGFP: AAV-GFP) into adult SST-cre mice and, after >3 weeks of viral incorporation, subjected them to 4d MD (Fig. 2e). In adult mice with SST-specific Lypd6 overexpression that

underwent 4d MD (SST-Lypd6 4d MD) there was a significant OD shift compared to non-deprived (no MD) counterparts (SST-Lypd6 no MD) or control 4dMD mice injected with AAV-GFP (SST-GFP 4d MD) (Fig. 2f). To test whether glutamatergic overexpression of Lypd6 would also induce plasticity in adult mice, we injected a viral cocktail of AAV-CamKII-cre with either AAV-Lypd6 or AAV-GFP into V1 of adult WT mice and, after >3 weeks, subjected them to 4d MD (Fig. 2e). The viral cocktail approach resulted in 93.2% of successfully co-transfected (GFP-positive) cells as positive for the excitatory cell marker vGlut1 (Supplementary Fig. 1c.), and 52.2% of total vGlut1-positive population as GFP-positive (Supplementary Fig. 1d). We did not observe a significant shift in OD in mice with glutamatergic overexpression of Lypd6 that underwent 4d MD (CamKII-Lypd6 4d MD) or in either of control counterparts (CamKII-Lypd6 no MD and CamKII-GFP 4dMD) (Fig. 2f). The cumulative distributions of ODI also show only a significant shift in the SST-Lypd6 4d MD mice (Fig. 2g). Lastly, comparisons of CBI scores show a significant decrease only in the SST-Lypd6 4d MD mice (Fig. 2h). Altogether, robust plasticity was measured only in the deprived mice that were overexpressing Lypd6 specifically in SST interneurons. These results suggest that SST interneurons are critical for Lypd6-mediated reactivation of plasticity in adult V1. Furthermore, the temporal and spatial restrictions of viral injections imply that overexpression of Lypd6 directly in V1 after the closure of critical period plasticity is sufficient for the induction of robust plasticity in adulthood.

α2 nicotinic acetylcholine receptor subunit is required for reactivation of ocular dominance plasticity

We next aimed to determine the nAChR subtype required for reactivation of V1 plasticity mediated by Lypd6 in SST interneurons. In the hippocampus the SST-positive oriens-lacunosum moleculare (O-LM) interneurons, which are physiologically similar to a subpopulation of cortical SST-expressing Martinotti interneurons [48], express Lypd6 as well as α2-subunit-containing nAChR (nAChRα2), which is the most sparsely expressed nAChR subtype in the brain and features a unique

non-desensitizing characteristic [39,42]. In the cortex, the punctate expression pattern of nAChRα2 subunit concentrated in deep cortical layers [49] highly resembles that of cortical Lypd6 [42]. Indeed, *in situ* hybridization for *Lypd6* and *Chrna2* mRNA revealed that 79% of nAChRα2-positive cells also express Lypd6, and that nAChRα2 subunit is expressed on more than 53% of Lypd6-positive cells (Fig. 3a-c). Furthermore, while 23% of SST-positive cells overlapped with cells expressing nAChRα2, 95% of nAChRα2-positive cells overlapped with SST-positive cells (Fig. 3 d-f). Consistent with a recent single cell RNA sequencing study in adult V1 [50], no overlaps were observed between nAChRα2 and VIP or vGlut1 – the markers of vasoactive intestinal peptide-expressing interneurons and pyramidal cells (data not shown). Together this confirms strong preferential co-expression of Lypd6 and nAChRα2 in a subpopulation of SST interneurons.

Due to this high degree of co-localization between Lypd6, a modulator of non-α7 nAChRs [43], and nAChRα2 we examined whether ablation of nAChRα2 could eliminate ocular dominance plasticity induced by SST-specific overexpression of Lypd6. To accomplish this, we created a bigenic SST-cre/Chrna2KO mouse line to allow SST-specific Cre-recombinase expression on a background of *Chrna2* knockout (Chrna2KO: α2KO) [51]. We then injected AAV-Lypd6 into V1 of adult SST-cre/α2KO bigenic mice, allowed >3 weeks for viral incorporation, and assessed ocular dominance plasticity after 4d MD (Fig. 3d). Intriguingly, ablating nAChRα2 (SST-Lypd6/α2KO 4d MD) eliminated the robust plasticity induced through SST-specific Lypd6 overexpression in adult V1. Unlike the adult SST-Lypd6 4d MD mice, adult SST-Lypd6/α2KO 4d MD mice as well as deprived and non-deprived adult α2KO mice (α2KO 4d MD and α2KO no MD) did not show significant shifts in OD (Fig. 3e), cumulative distributions of ODI (Fig. 3f), or significant decreases in CBI (Fig. 3g). These findings strongly suggest the requirement of nAChRα2 in the induction of plasticity by Lypd6 in SST interneurons.

To further investigate the physiological role of nAChRα2 in regulating plasticity in adult V1, we turned to a condition known for modulating SST interneuron activity as well as reactivating V1 plasticity. Voluntary physical exercise through the use of a running wheel was recently shown to induce juvenile

form of plasticity in adult mice [52]. Interestingly, locomotion is also known to modulate SST interneuron activity [29-33]. We therefore examined the functional contribution of nAChRα2 in this model of adult reactivation of V1 plasticity. When allowed voluntary exercise (+Running) on a running dish during the 4d MD (Fig. 3h), adult WT mice (WT 4d MD, +Running) displayed a significant shift in ocular dominance, consistent with the aforementioned published study [52]. However, adult α2KO mice subjected to the same condition (α2KO 4d MD, +Running) did not show significant shifts in OD (Fig. 3i), cumulative distributions of ODI (Fig. 3j), or significant decreases in CBI (Fig. 3k). In addition, SST-specific viral knockdown of Lypd6 in the adult V1 of did not block voluntary-exercise-induced plasticity and was no different from adult WT 4d MD+Running mice (Supplementary Fig. 2). We postulate that other members of the Lynx family played a compensational role in mediating voluntary-exercise-induced plasticity in the Lypd6 knockdown context. Alternatively, as Lypd6 is a positive modulator of non-α7 nAChRs, and given that knocking out *Chrna2* eliminates the voluntary-exercise-induced plasticity, simply knocking down *Lypd6* may be insufficient for blocking exercise induced-plasticity in the presence of nAChRα2. Finally, we performed qPCR on V1 extractions of adult WT 4d MD+Running mice (n=4) and control adult WT 4d MD (n=4) mice in order to examine whether voluntary exercise changes the expression of *Chrna2* or *Lypd6*, but did not find any significant differences (*Chrna2*: P=0.7908, *Lypd6*: P=0.7111 Student's t-test). We speculate that perhaps increased cholinergic activity is sufficient to enhance nAChRα2 signaling and encourage voluntary-exercise-induced plasticity in the adult brain. We also compared *Chrna2* expression between adult SST-Lypd6 no MD mice (n=2), and adult SST-GFP no MD mice (n=2), and did not find any significant differences (P=0.20, Student's t-test). Collectively, these results suggest that the voluntary-exercise-induced model of V1 plasticity requires nAChRα2, further signifying the critical role of nicotinic signaling through nAChRα2 in reactivating plasticity in adulthood.

Lypd6 expressed in SST interneurons increases their activity to drive ocular dominance plasticity

Having ascertained that the effect of Lypd6 in reactivating V1 plasticity is regulated through SST interneurons, we investigated the plasticity mechanisms in these cells as well as downstream circuits. Cortical SST interneurons are known to provide inhibitory local inputs onto PV interneurons [28,53-57] and inhibit them twice as potently they do pyramidal neurons in mouse V1[58]. As rapid reduction in PV interneuron firing during the first day of MD is a unique trigger of V1 plasticity during the critical period [22], we examined whether adult overexpression of Lypd6 in SST interneurons can increase their activity and in turn suppress PV activity during the first day of MD.

First, to directly evaluate how overexpression of Lypd6 in SST interneurons affects their activity, we used channelrhodopsin-2 (ChR2) as an optogenetic tag to allow identification of visually evoked cells as SST interneurons based on whether they can also be activated by optogenetic stimulation (Fig. 4a, b). We targeted expression of ChR2 specifically in SST interneurons by injecting AAV with Cre-dependent expression of ChR2 (AAV1-dflox-hChR2(h134R)-mCherry-WPRE-hGH: AAV-ChR2) into adult SST–Cre mice along with either AAV-Lypd6 (SST-Lypd6) or AAV-GFP (SST-GFP) and, after >3 weeks of viral incorporation, subjected the mice to 24 hours of monocular deprivation of the contralateral eye (1d MD) (Fig. 4c). Considering the physiological context of endogenous Lypd6 expression in deep cortical layers, we restricted our analyses to only the SST interneurons recorded from the lower half of the 16-channel linear silicone probe in an effort to focus on the SST interneurons of lower layer IV, layers V, and VI. In adult SST-Lypd6 mice that underwent 1d MD (SST-Lypd6 1d MD), there was a significant increase in the visually evoked firing rate of SST interneurons compared to 1d MD adult SST-GFP mice (SST-GFP 1d MD) or non-deprived adult SST-Lypd6 (SST-Lypd6 no MD) mice when statistically analyzed using a linear mixed model (LMM; for details See *Methods – Statistical analysis*) that considers “animal” as a variable with random effect, and “genetic manipulation” (-GFP or -Lypd6) and “experience” (1d MD or no MD) as variables with fixed effects (Fig. 4d, e). In comparing

baseline firing rates without visual stimulation, only a trending increase in firing rate was observed in SST-Lypd6 1d MD mice (4.47 spikes/sec) relative to SST-GFP 1d MD mice (2.87 spikes/sec) (SST-Lypd6 1d MD vs. SST-GFP 1d MD: P=0.057), and no significant difference was found when assessing experience-dependent effects (SST-Lypd6 1d MD vs. SST-Lypd6 no MD (4.77 spikes/sec): P=0.97, LMM). This result suggests an interactive effect of Lypd6 overexpression and sensory experience in rapidly increasing SST interneuron activity.

To then determine the causal role of rapid increase in SST interneuron activity itself in mediating plasticity, we examined if chemogenetic activation of SST interneurons strictly during the first day of monocular deprivation alone can reactivate plasticity (Fig. 4f and Supplementary Fig. 3). Adult SST-cre mice were injected with an AAV with Cre-dependent expression of excitatory Gq protein-Designer Receptors Exclusively Activated by Designer Drugs (AAV8-hSyn-DIO-hM3D(Gq)-mCherry: AAV-GqDREADD)[59]. In mice given Clozapine-N-Oxide (CNO), to activate SST interneurons during the first day of the 4d MD (CNO+), there was a significant OD shift compared to mice that received control saline injections (CNO-) (Fig. 4g). The cumulative distributions of ODI show a significant shift in CNO+ mice compared to CNO- mice (Fig 4h). Comparisons of CBI scores show a significant decrease only when SST interneurons were activated by injection of CNO (Fig. 4i). Together, these results imply a novel role for SST interneuron activity in reactivating a juvenile form of plasticity in adult V1.

Lypd6 expressed in SST interneurons suppresses PV interneuron activity to drive ocular dominance plasticity

Finally, we aimed to elucidate the consequence of Lypd6-mediated elevation in SST activity upon PV interneuron activity. In adult SST-cre mice, we injected AAV-Lypd6 (SST-Lypd6) or AAV-GFP (SST-GFP) and, after >3 weeks of viral incorporation, subjected the mice to 1d MD (Fig. 5a). We putatively determined the cell type identity of visually evoked PV interneurons using spike shape-based classification. Visually evoked cells were sorted into two categories: putative fast-spiking PV (pFS)

neurons defined by a narrow spike waveform that is an electrophysiological characteristic unique to PV interneurons, or regular-spiking neurons (RS) (Supplementary Fig. 4d, e).

In adult SST-Lypd6 mice that underwent 1d MD (SST-Lypd6 1d MD), LMM showed a trending reduction in pFS neuron firing rates with no statistical significance compared to all control groups (Fig. 5b, c), likely reflecting a broad distribution of firing rates among pFS neurons. As it appeared that less pFS neurons of higher visually evoked firing rates were observed after 1d MD in adult SST-Lypd6 mice, we systematically binned normalized firing rates to determine the largest separation of firing rates between adult SST-Lypd6 and SST-GFP groups and compared the fractions of pFS neurons with firing rates higher than the separation. Using one-way analysis of variance at animal level, we found a significant reduction in the fraction of pFS neurons of higher firing frequency in adult SST-Lypd6 1d MD mice (Fig. 5d). This suggests an experience-dependent drop in firing rate of PV interneurons when Lypd6 is overexpressed in adult SST interneurons. Furthermore, the distributions of pFS neuron firing rates that are broader than those of SST interneurons in our data suggest that sub-populations of PV interneurons may particularly be impacted by SST-specific Lypd6 overexpression. With respect to baseline firing rates, no significant differences were observed (SST-Lypd6 1d MD (2.06 spikes/sec) vs. SST-GFP 1d MD (2.55 spikes/sec): P=0.86, vs. SST-Lypd6 no MD (3.08 spikes/sec): P=0.49, LMM). Altogether these results may suggest an interactive effect of overexpression of Lypd6 and sensory experience in rapidly decreasing PV interneuron activity.

To determine the causal role of PV interneuron activity in robust plasticity regulated by Lypd6, we examined if chemogenetic restoration of PV interneuron activity during the first day of deprivation can prevent robust plasticity regulated by Lypd6 overexpression (Fig. 5d and Supplementary Fig. 4). We created a bigenic Lypd6Tg/PV-cre mouse line to allow PV-specific Cre-recombinase expression on a background of pan-neuronal Lypd6 overexpression. Adult Lypd6Tg/PV-cre mice were injected with AAV-GqDREADD. In mice injected with CNO to activate PV interneurons during the first day of the 4d MD (CNO+), there was a significant blockage of ocular dominance plasticity compared with mice that

received control saline injections (CNO-) (Fig. 5g). The cumulative distributions of ODI show that the shift is significantly eliminated in CNO+ mice compared to CNO- mice (Fig. 5h). Comparisons of CBI scores show a blockage of decrease only in CNO-injected mice where PV interneurons were activated (Fig. 5i). While we cannot fully rule out the possibility that the suppression of V1 responses by chemogenetic activation of PV interneurons partly contributed to the blockage of plasticity, together these results implicate the role of Lypd6 in potentiating SST activity to engage an SST interneuron-based inhibition of PV interneurons – a novel inhibitory-inhibitory microcircuit, to induce a juvenile form of plasticity in the adult V1.

Discussion

Our study identifies an endogenous nAChR modulator, Lypd6, and its action through nAChRα2 as the first targetable SST interneuron-specific molecular mechanism for reactivating plasticity in the adult cortex. As SST interneurons are known to be modulated by alteration of visual inputs [27], neuromodulation induced by locomotion [29-33], and top-down regulation [34-36], the Lypd6-nAChRα2 system is ideally situated to gate these multiple modulatory inputs onto SST interneurons to regulate plasticity. Having demonstrated the Lypd6-nAChRα2 system as a molecular target for restoring plasticity in the adult brain, it would be necessary for future studies to first investigate the mechanistic details of the action of Lypd6 on nAChRα2 in SST interneurons, and then determine to what extent this system is relevant in regulating plasticity in the juvenile cortex. Finally, our study provides critical knowledge underlying the molecular and circuit means for the induction of plasticity in the adult visual cortex, which can unveil insights into establishing new therapeutic targets and strategies for treating disorders where potential for recovery is limited due to diminished plasticity. Therefore it is imperative for future long-term efforts to aim towards the development of agonists with high specificity for nAChRα2 to test as drug candidates in disease models such as one for amblyopia.

Lypd6, like several members of the Lynx family [41], is membrane tethered through a glycophosphatidylinositol (GPI)-anchor and is known to positively modulate nicotinic signaling [43]. Our results from SST interneuron-specific *Lypd6* overexpression on a background of *Chrna2* knockout suggest that the primary mechanism for Lypd6-based initiation of plasticity is mediated specifically through nAChRα2s. However, Lypd6 may also mediate additional mechanisms unrelated to nicotinic signaling [60]. While the subcellular localization of Lynx proteins has not been fully elucidated, there are evidences that show they potentially localize to synaptic compartments to modulate nAChRs [61] [62]. Lypd6 may facilitate the activation of SST interneurons by impacting postsynaptic nicotinic modulation of excitatory synaptic input onto SST interneurons, such as in the case of hippocampal CA1 O-LM interneurons where nAChRα2 and their non-desensitizing features are critical for gating LTP through receptor-mediated calcium influx [39]. Alternatively, Lypd6 may modulate nicotinic signaling at presynaptic SST terminals to facilitate the release of GABA [63]. Nevertheless, either potential mechanism may achieve the facilitation of SST interneuron activity – physiological condition that we confirmed, through chemogenetic activation of SST-interneurons, to be a trigger of robust plasticity (Fig. 4). Proper antibodies suited for immunohistochemical analyses of Lypd6 and nAChRα2 are both currently unavailable. However, future studies may benefit by applying recently developed technologies, such one that uses *in vivo* genome editing [64] to label endogenous Lypd6 or nAChRα2 protein and visualize them at resolutions as high as the synaptic level. Such method would reveal finite details regarding their interaction as well as any other endogenous mechanisms governed by Lypd6.

Our study highlights Lypd6- and nAChRα2-expressing SST interneurons located in deep layers of V1 as a key cellular target for reactivating plasticity in adulthood through nicotinic neuromodulation. Previous studies have reported mixed results regarding the question of whether nicotinic signaling directly affects SST interneurons. While some studies reported clear nicotinic responses in neocortical

SST interneurons [65] [66] [28], some have reported otherwise [67] [68]. This discrepancy may reflect the observation that expression of Lypd6 and nAChRα2 is selectively expressed in a subpopulation of SST interneurons located in deep cortical layers (layers 5 and 6) but not of those in layer 2/3 [50] [42]. It is possible that such a minor subpopulation of deep layer Lypd6-expressing SST interneurons was not well represented in the previous negative reports. For example Gulledge *et al.*[66] reported that 30% of SST interneurons in layer 5 rat V1 responded to nicotine, which is consistent with the percentage of SST cells expressing Lypd6 and nAChRα2 (Fig. 3). While the expression of Lypd6 and nAChRα2 are limited to a subpopulation of deep layer cortical SST interneurons, the unique non-desensitizing nature of nAChRα2 allows continual activation and calcium entry in the presence of Ach [39], making the nAChRα2 highly suited for driving cortical plasticity through elevation of nicotinic tone with Lypd6 or by receiving cholinergic inputs through locomotion. The SST-interneurons in deep cortical layers are also reported to project widely to almost all cortical layers and types of neurons [69], which can potentially contribute to widespread distribution of the drive for cortical plasticity exerted through nAChRα2. Overall our study highlights the SST interneuron that expresses Lypd6 and nAChRα2 as a cellular target of nicotinic neuromodulation for reactivating cortical plasticity in the adult V1. More mechanistic insight into the physiological action of ACh and Lypd6 on nAChRα2 signaling can be expected in future studies by taking full advantage of the recently developed mouse lines with selective expression of Cre recombinase in subpopulations of SST interneurons [38] [70]. This should be combined with future development of a new ChAT-ChR2 transgenic mouse line that avoids abnormally high endogenous cholinergic tone [71], to allow proper optogenetic modulation of endogenous Ach release. Finally, as our study resonates with the current understanding of the profound functional diversity of SST interneurons that has been steadily developing in recent years, we anticipate an impetus for development of selective nAChRα2-selective antagonists for acute pharmacological modulation, for they would become crucial tools for further investigating the functional role of the subpopulation of nAChRα2-expressing SST interneurons in the cortical circuit.

Our findings establish a novel circuit mechanism – SST interneuron-mediated inhibition of PV interneurons, for triggering a juvenile form of plasticity in adulthood. To our knowledge, this is the first evidence implicating the role of the SST-PV disinhibitory microcircuit in modulating cortical plasticity. We demonstrated that the overexpression of Lypd6 in SST interneurons leads to reduced activity in sub-population of PV interneurons, similar to what is typically observed specifically in juvenile mice after 1 day of visual deprivation [22]. Interestingly, a recent study showed that *silencing* SST interneurons for the *entirety of 5 days of visual deprivation* could induce some level of cortical plasticity in adulthood. However the nature of plasticity measured in that study was that of an adult form, characterized by an elevation of open ipsilateral eye response but no reduction of the deprived contralateral eye response - the latter is required to define a juvenile form of plasticity [26]. Nevertheless, collectively these studies highlight the capabilities of SST interneurons in engaging both a homeostatic adult form of plasticity [26] and a rapid form of juvenile like-plasticity [22], depending on the level of SST interneuron activity (reduced or enhanced) and the timing of activity change (during the initial phase within 1 day or later homeostatic phase after 5 days). This reflects the placement of the SST interneuron in the cortical circuit as a versatile integrator of a variety of inputs. Consistently, recent studies demonstrated that SST interneurons in V1 could either be activated or suppressed by neuromodulation triggered by locomotion depending on the context of the visual environment [29-33]. Specifically, locomotion enhances overall SST interneuron activity when the mouse is presented with large visual input[29,30] including a full-field gray screen [31]. On the other hand, SST interneurons are largely non-responsive to small visual inputs [30] or are suppressed in darkness by the inhibitory action of the VIP interneurons [29 32]. Here in our study we propose a model whereby the Lypd6-nAChRα2 system may function as a molecular switchboard for SST interneurons to shift modes and activate the SST-PV disinhibitory circuit [38,72]. This mechanism then serves to trigger a juvenile form of plasticity [22] while suppressing an adult form of plasticity mainly through reduction of inhibitory action of SST interneurons upon the distal dendrites of

pyramidal neurons [26,73,74] that would normally be engaged through an nAChRα2-independent VIP-SST disinhibitory circuit [26]. In this model, both SST-PV and VIP-SST disinhibitory circuits can co-exist to play complementary roles in the modulation of plasticity, depending on the context and states of the adult brain. While SST interneurons are known to exhibit maturation towards the end of the critical period in V1[75], the differential contributions of SST-PV and VIP-SST circuits in regulating plasticity between critical period and adulthood remains unknown. It also remains to be determined how neuromodulation of SST interneurons change from critical period to adulthood to regulate plasticity.

The potential for signaling through nAChRα2 and its modulation by Lypd6 to induce plasticity in the adult cortex opens up the possibility of targeting this receptor for therapeutic interventions. The selective expression of both Lypd6 and nAChRα2 in SST interneurons make them attractive novel therapeutic targets with the potentially fewer off target effects [76-78] than interventions directed against more non-specific targets (e.g. more abundant nicotinic subunits), which are ideal for treating conditions such as amblyopia, stroke, and traumatic brain injury where hope for recovery is thin due to diminished plasticity. There have been recent reports of positive allosteric modulators with significantly higher specificity for nAChRα2 [76-78] that could serve in future studies as promising drug candidates to test in animal models of amblyopia. Combinations of such potential pharmacological interventions with behavioral interventions like physical exercise [52] known to impact SST interneuron activity [29-32,79] (Fig. 3) may also be fruitful. Finally, our study highlights the disruption of cortical plasticity as a key pathophysiological consequence of mutations of the *nAChRα2* gene and its non-coding regulatory elements [80 81 82 83], or deficits in SST interneurons[84 85 86 87 88 89 90], which have been commonly reported among multiple neurodevelopmental, neurodegenerative, and psychiatric disorders including epilepsy, addiction, depression, and schizophrenia.

Methods

Animals

All mice were housed in groups of 2–5 together with the sibling groups of the same sex in standard and uniform cage sizes (199 mm x 391 mm x 160 mm: width x depth x height, GM500, Tecniplast) under a 12hr light:dark cycle (lights on at 7:00AM: lights off at 7:00PM) in a facility with constant temperature (23°C) and ad libitum access to food and water. Wild-type C57Bl/6 mice were obtained from Jackson laboratory and Charles River. Both male and female were used. Lypd6Tg mice were originally generated by A.Z.[43], and transferred to H.M. and back-crossed to C57Bl/6. Somatostatin-ires-cre (SST-cre: Jackson laboratory #013044), Parvalbumin-ires-cre (PV-cre: Jackson laboratory #008069), and Chrna2KO (MMRRC #30508) were purchased and bred in-house. Bigenic lines were created through targeting breeding of above strains. All animal protocols were approved by the Institutional Care and Use Committee (IACUC) at Icahn School of Medicine at Mount Sinai.

Monocular deprivation

Monocular deprivation procedure for animals that underwent either 4 day or 1 day of monocular deprivation was conducted on the contralateral eye and with ipsilateral eye left open. The mice were anesthetized with isoflurane during the entire procedure. Eyelid margins were trimmed using an iris scissor and one eye was sutured closed for one or four days. Following MD, mice were returned to their home cage prior to extracellular recording and subsequent euthanasia.

Generation and validation of AAV-Lypd6 and AAV-miR-Lypd6

Lypd6 was amplified from a cDNA library derived from whole mouse V1, subcloned into a pcDNA3.1 (-) vector. Two oligonucleotides including shRNA sequence for Lypd6 (TGCTGAATGACAGAGATGCTGTTCCCGTTTTGGCCACTGACTGACGGGAACAGTCTCTGTCATT,C

CTGAATGACAGAGACTGTTCCCGTCAGTCAGTGGCCAAAACGGGAACAGCATCTCTGTCATTC, life technologies) previously reported to knockdown *Lypd6* expression [43] were subcloned into pcDNA6.2-GW/EmGFP-miR using BLOCK-iT Pol II miR RNAi Expression Vector Kit with EmGFP (life technologies). Subclonings were performed using an isothermal DNA assembly method (Gibson Assembly; New England Biolabs) and transformed into *E. Coli*. Colonies with correct insert were identified through DNA sequencing (Genewiz), cultured and then isolated using a Hi-speed Midiprep kit (Qiagen). Expression was first examined by transfection of N2A cells *in vitro*. To create pAAV vector, an inverted bicistronic 2A sequence was inserted into pAAV-Ef1α-DIO-EGFP-WPRE-pA (Addgene#37084) upstream of EGFP by PCR linearization and overhang production on pAAV vector. The pcDNA3.1(-)-Lypd6 vector was used as a template for the Lypd6 insert which was subsequently inserted into the pAAV-DIO-EGFP-2A vector as described above to create a pAAV-DIO-EGFP-2A-Lypd6-WPRE-pA vector. pcDNA6.2-mGFP-miR-Lypd6 vector was subcloned into pAAV-DIO-EGFP-2A-Lypd6-WPRE-pA vector to generate pAAV-DIO- mGFP-miR-Lypd6 (pAAV-miR-Lypd6) vector. After sequence verification, a large culture and Maxiprep isolation produced a purified vector that was sent to the UNC viral core for viral packaging using an AAV8 serotype. To confirm viral efficiency, AAVs were stereotaxically injected (see below for injection methods) into V1 of SST-cre mice. After perfusion, sections were labeled with rabbit anti-somatostatin antibodies (1:1000; Peninsula Laboratories) and the SST interneuron-specific GFP expression was confirmed. V1 was micro-dissected from an additional cohort of mice to assay overexpression or knockdown of Lypd6 through qPCR. RNA was isolated using an RNeasy lipid tissue mini kit (Qiagen) and cDNA was produced. The cDNA was subjected to qPCR analysis using a Taqman assay (Life Technologies) at the Icahn School of Medicine at Mount Sinai Quantitative PCR CORE facility.

Stereotaxic injection

Mice were isoflurane anesthetized and head-fixed in a mouse stereotaxic apparatus (Narishige). A mid-line incision was made in the scalp and a micro-drill was used to drill a small hole in the skull over the right visual cortex. Three injections (0.5 µl each) were made into the deep layers of V1 binocular zone (from lambda: AP: 0.0, ML: 3.1, DV: 0.6; AP: 0.0, ML: 2.85, DV: 0.6; AP: 0.3, ML: 3.0, DV: 0.6) using a 2.5 µl syringe (Hamilton Company) with a 30-gauge needle and microsyringe pump controller (World Precision Instruments) set to inject at 200nl/minute. The syringe remained in place for one minute following injection to reduce backflow of virus. After injections, the skull hole was sealed using Kwik-Sil (World Precision Instruments), and the scalp was sutured. The mice were allowed to recover from anesthesia in an empty cage over a warming pad. Following recovery, mice were returned to their home cage where they remained for >3 weeks to allow for viral incorporation prior to any additional procedures or testing. The following viral constructs were used in this study: AAV-Lypd6 (AAV8-EF1α-DIO-EGFP-2A-Lypd6), AAV-GFP (AAV8-hSyn-DIO-EGFP) (University of North Carolina (UNC) Vector Core), AAV-CamKII-Cre (AAV8-CamKIIa-mCherry-Cre: UNC Vector Core), AAV-GqDREADD (AAV8-hSyn-DIO-hM3D(Gq)-mCherry: UNC Vector Core), AAV-ChR2 (AAV1-Ef1α-dflox-hChR2(H134R)-mCherry-WPRE-hGH: Penn Vector Core), AAV-miRLypd6 (AAV8-Ef1α-DIO-EGFP-2A-miRLypd6), and AAV-hSyn-Cre (AAV8-hSyn-mCherry-Cre: UNC Vector Core).

Chemogenetic activation of hM3d(Gq) Designer Receptors Exclusively Activated by Designer Drugs (DREADD)

Clozapine-N-Oxide (CNO; Sigma-Aldrich), a normally inert compound that specifically activates DREADD receptors, was prepared in 0.9% saline and injected i.p. into adult SST-Cre (Fig. 4f-i) or Lypd6Tg/PV-cre bigenic mice (Fig. 5d-g) at a concentration of 3 mg/kg. CNO or saline was injected immediately following MD and again 12 hours later for DREADD induced activation of SST or PV interneurons during the first day of MD following the previously validated protocol in mouse visual cortex[22](Supplementary Fig. 3, 4).

In vivo extracellular recording

As previous described, preparatory surgery leading to, and recording itself was performed initially under nembutal/ chlorprothixene anesthesia and then maintained with isoflurane [46]. For animals that underwent either 4 days or 1 day of monocular deprivation, the deprived (contralateral) eye was reopened just prior to the start of recordings. Visually evoked single-unit activity were recorded in response to a high contrast single bar, generated by Visage System (Cambridge Research Systems), that laterally traveled across the monitor in a 4 second interval followed by a 6 second interstimulus interval per trial. Through the use of an eye patch, the stimulus was separately presented to the contralateral eye and then to the ipsilateral eye for at least 12 trials each. For each animal, 3 to 10 single units were recorded in each of the 4 to 6 vertical penetrations spaced evenly (250 μm intervals) across mediolateral extent of V1 to map the monocular and binocular zones to avoid sampling bias. A linear 16-channel electrode was used to record each vertical penetration, which allowed recording from upper (channels 1~8) and lower (channels 1~9) cortical layers with similar weight. By analyzing 7 of the experimental groups that were used in our data, we found that the fraction of neurons recorded from upper layers (0.5235 ± 0.02350) did not differ from that of neurons recorded from lower layers (0.4765 ± 0.02350) (n=35 animals: P=0.3247, Student's t-test for paired samples). The signal was amplified and thresholded (OmniPlex, Plexon). To ensure single-unit isolation, the waveforms of recorded units were further examined offline (Offline Sorter, Plexon). To analyze the electrophysiology data, normalized OD index of single neuron was computed by custom made MATLAB program by peristimulus time histogram analysis of peak to baseline spiking activity in response to each eye: {[Peak(ipsi)-baseline (ipsi)]–[Peak (contra)-baseline(contra)]}/{[Peak (ipsi) – base line(ipsi)]+ [Peak(contra)-baseline(contra)]}.). OD scores were converted from OD index using a 7-point classification scheme as follows: -1 to -0.5 = 1, -0.5 to -0.3 = 2, -0.3 to -0.1 = 3, -0.1 to 0.1 = 4, 0.1 to 0.3 =5, 0.3 to 0.5 =6, 0.5 to 1 =7. For each binocular zone, contralateral bias index (CBI) is calculated according to the formula:

[(n1-n7)+2/3(n2-n6)+1/3(n3-n5)+N]/ 2N, where N=total number of cells and nx=# of cells corresponding to OD score of x.

For optical tagging experiments, SST interneurons were optogenetically tagged by injecting a Cre-dependent virus expressing channelrhodopsin-2 (AAV1-Ef1α-dflox-hChR2(H134R)-mCherry-WPRE-hGH: Penn Vector Core) into the V1 binocular zone of SST-cre mice. The expression of channelrhodopsin in a cell type of interest allowed the use of optogenetic stimulation with a blue light as a search stimulus to simultaneously sort stimulus-locked responses from cell types of interest, and then record their visually evoked responses, by using an optic fiber-coupled 16-channel linear silicone probe (Neuronexus). This allowed accurate and high-throughput recordings of specific cell types, even against broad baseline noise and activities of other neuronal populations. Optogenetically tagged SST interneurons of the V1 binocular zone were identified using a 473 nm (blue) laser search stimulus emitted and delivered through the optic fiber coupled to the silicone probe and oriented immediately above the V1 cortical surface. After sorting for optogenetically responsive units (SST interneurons expressing ChR2), the optogenetic stimulus was switched off. Then a high-contrast single bar visual stimulus was presented to each eye to record the visual evoked responses (spike firing rate) of the sorted units. Analysis of visually evoked activities of sorted SST interneurons were restricted to only those recorded from the lower half of the 16-channel linear silicone probe in an effort to focus on the SST interneurons of lower layer IV, layers V, and VI. All animals with less than 10 analyzable lower layer SST interneurons recorded were excluded from the analysis. Normalized firing rate of each lower layer SST interneuron, in response to contralateral eye (or deprived eye in animals in 1 day monocular deprivation groups) stimulation, was computed by first using a custom made MATLAB program by generating a peristimulus time histogram-based analysis of peak and baseline spiking activity in response to visual stimulus. The peak visually evoked activity through contralateral/deprived eye stimulation was then subtracted by baseline spiking activity in order to obtain the normalized visually evoked firing rate.

To isolate visually evoked responses from putative fast-spiking (pFS) neurons, visual stimulus responsive cells were distinguished as pFS neurons or regular-spiking (RS) neurons by means of spike width- (trough-to-peak time) based classification. The spike-width criterion for separating into pFS and RS neurons was established by measuring the spike width of optogenetically tagged PV interneurons. PV interneurons were optogenetically tagged by injecting a Cre-dependent virus expressing channelrhodopsin-2 (AAV1-Ef1α-dflox-hChR2(H134R)-mCherry-WPRE-hGH, Penn Vector Core) into V1 binocular zone of PV-cre mice. During recording, pFS neurons were first identified and sorted, using a 473 nm laser search stimulus delivered through the optical fiber coupled to the 16-channel silicone probe and oriented immediately above the V1 cortical surface, depending on their responsiveness to blue light stimulation within 3 msec post blue light emission. The search stimulus was then exchanged to a visual stimulus. Visually evoked spike widths of the pFS neurons identified by optical tagging were then pooled to establish the official criterion for pFS neurons as having visually evoked spike width time (trough-to-peak time) of less than 412 μsec (Supplementary Fig. 4). Averaged spike waveform data for each unit was analyzed using a custom made MATLAB program to obtain a spike width time for each unit. All pFS neurons sorted and recorded were included in the analysis of their visually evoked activity. All animals with less than 10 analyzable pFS neurons recorded were excluded. Using the same method for analyzing SST interneurons, normalized firing rates of pFS neurons were calculated from responses to contralateral/deprived eye stimulation.

Following recordings, all AAV injected mice were transcardially perfused and the extent of GFP or mCherry signal was utilized to assess the viral transduction. Only mice that exhibited GFP or mCherry signal in the recorded V1 area were included for the analysis of ocular dominance plasticity or SST/pFS neuron activity. The experimenters performed while blind to experimental conditions such as viral constructs or CNO/saline administration, but not monocular deprivation.

In situ hybridization

The production of probes and methodology for *in situ* hybridization has been previously described[42]. Briefly, RNA probes including a fluorescein or digoxinogen (DIG) tag were generated and utilized to label *Lypd6, SST, VIP vGlut1, GFP,* and *Chrna2* mRNA in 7 μm sections of V1 from fresh frozen brains of animals at P28 (CP) and >P60 (adult). To fluorescently label mRNA, anti-fluorescein/DIG-POD (1:2000; Roche) and anti-fluorescein/DIG-Alkaline phosphatase (AP) (1:1000; Roche) antibodies were used. POD-conjugated antibody labeling of mRNA was proceeded with with TSA Plus DNP signal amplification (Perkin Elmer) and a subsequently labeling with anti-DNP-KLH-488 antibodies (1:1000; Life Technologies). AP-conjugated-antibody-labeled mRNA was stained using HNPP/Fast Red (Roche). Imaging was performed using an LSM780 confocal microscope (Zeiss). ImageJ was used to quantify the density of labeled pixels from each image or to examine co-localization using a color based thresholding method. For the quantification of Lypd6 *mRNA* expression across age in V1, pixel density (>2 standard deviations above mean intensity of full image field) was determined from low magnification images of V1 binocular zone using ImageJ software. For the quantification of co-localization of *Lypd6* or *SST* or *VIP* with *nAChRα2*, the number of cells positive for *Lypd6/SST/VIP* or *nAChRα2* in each image was determined using ImageJ by automated counting using a threshold of >2 standard deviations above background and limiting to particles of >40 μm cell diameter. To calculate the co-localization percentage, first color based thresholding was utilized in ImageJ to isolate and quantify the co-localized cells, then percentage was calculated by dividing the number of co-localized cells by the number of *Lypd6/SST/VIP* or *nAChRα2* positive cells in each image. For the quantification of co-localization of *GFP* and *vGlut1* mRNA, thresholding was first utilized to isolate and calculate number of particles representing *GFP* labeled cells (>40 μm cell diameter). Then the corresponding *vGlut1* labeled image was redirected to the mask retained from the analysis of *GFP* labeled image to calculate total number and then percentage of *GFP* labeled cells with co-localized *vGlut1* labeling. For the quantification of *Lypd6* mRNA expression in V1 binocular zone of mice injected with a cocktail of AAV-Lypd6 and AAV-CamKII-Cre, low magnification images of binocular V1 from the injected or the corresponding naïve hemisphere were analyzed for particles after thresholding. Absolute

intensity for each particle was then measured as the product of mean intensity and area of particle. All absolute intensity values were summed to obtain total binocular V1 intensity, which was subsequently normalized by dividing by the μm^2 area of the V1 binocular zone. The V1 binocular zone of each image was assessed using Paxinos and Franklin's The Mouse Brain in Stereotaxic Coordinates (1997) as reference.

Quantitative PCR (qPCR)

Adult mice were deeply anesthetized with isoflurane, checked for response with paw pinch, and decapitated. The brain was extracted, and under RNAse- free conditions, briefly washed in ice cold 0.1 M phosphate buffer, and then an estimated area of cortical tissue representing V1 – a 2mm-by-2mm area of the cortex most posterior and 2mm lateral from the median, was cut out, white matter removed, immediately frozen on dry ice, and stored under -80°C. Total RNA was extracted from V1 using the RNeasy Mini Kit (Qiagen) and stored at -80°C. concentrations of total V1 RNA yielded ranged from 0.22 to 0.3 µg/µl. Total V1 RNA was converted to cDNA using a High- Capacity cDNA Reverse Transcription Kit (Life Technologies). qPCR was performed at the Mount Sinai Quantitative PCR core facility using 7900HT Real-Time PCR instrument (ABI/Life Technologies), TaqMan probes (catalog numbers: *Lypd6* Mm00622636_01, *Chrna2* Mm00460630_m1, ABI/Life Technologies) and TaqMan Universal Master Mix II, no UNG (ABI/Life Technologies). Quantification of the fold change was calculated via the –ΔΔCT method (equivalent to a log2 fold change), using ΔCT values derived by normalization of CT values to mouse beta actin as reference housekeeping gene.

Immunohistochemistry

Anesthetized mice were transcardially perfused with cold 4% paraformaldehyde (PFA) dissolved in 0.1M phosphate buffer. The brains were post-fixed in 4% PFA at 4 °C, and cryoprotected in 30%

sucrose solution. The frozen brains were sectioned into 30-µm-thick coronal sections using a cryostat (CM3050, Leica). Free-floating sections were washed in tris-buffered saline (TBS), pH 7.5, and then blocked in 1% bovine serum albumin in TBST (0.25% Triton X-100 in TBS) for 1 h. The sections were incubated with mouse anti-parvalbumin (1:500; Swant), rabbit anti-somatostatin (1:1000; Peninsula Laboratories), or rabbit anti-c-Fos (1:500; Calbiochem) antibodies overnight at room temperature. After primary antibody incubation the slices were washed in TBST, followed by secondary antibody incubation with Alexa fluor dyes (Thermo Fisher Scientific). Imaging was performed using a Zeiss LSM780 confocal microscope at 20 or 40X magnification. The investigator performing the analysis was blind to the animal genotype.

Statistical analysis

The following statistical approaches were utilized for experiments assessing ocular dominance plasticity. χ^2 test was used to compare at cell level distributions of ocular dominance scores between two groups and assess for ocular dominance shift. For readability, the histogram figures for distribution of ocular dominance scores (OD Scores) represent percentage of cells rather than actual cell number. However the χ^2 statistics are results of the tests conducted on actual cell number. Cumulative distributions of ocular dominance index (ODI) were compared at cell level by using the Kolmogorov-Smirnov (K-S) test. One-way analysis of variance (ANOVA) was used to compare contralateral bias index (CBI) at animal levels and Tukey's multiple comparisons test was used for post hoc analyses. As justification of the use of a parametric test, normality of the CBI data was tested by using the D'Agostino-Pearson Test and Shapiro-Wilk Test on any groups where n=mice exceeding the criteria for the tests (n>8, and n>7 respectively). Normality was confirmed in all groups where tests were applicable: WT MD, WT no MD, Lypd6Tg 4d MD, and SST-Lypd6 4d MD. In addition, we applied the Shapiro-Wilk Test to the CBI data of a key experimental group from our previous study (Smith *et al.*, 2016) that utilized the same experimental design and statistical analyses for testing ocular dominance

plasticity, and also confirmed normality. Initial comparison of pFS cell (PV interneuron) and SST interneuron firing rates were conducted using one-way ANOVA with Bonferroni corrected multiple comparison tests for post hoc analyses. To officially determine the statistical significance of differences in SST and PV interneuron firing rates, a linear mixed modeling (LMM) approach was used, from packages LmerTest (v. 2.0.32), lme4 (v. 1.1.12), and lsmeans (v. 2.25) in the R programing language (v. 3.2.2). This model considered "animal" as a variable with random effect, and "genetic manipulation" (-GFP or -Lypd6) and "experience" (1d MD or no MD) as variables with fixed effects. For further analysis of pFS neuron activity, the normalized firing rates were systematically binned into binary "high" and "low" firing rate categories by determining the firing rate value where the largest separation between the groups (SST-Lypd6 and SST-GFP) occurs. The fractions of pFS neurons of firing rate higher than the systematically determined separation point were then compared between groups at animal level using one-way ANOVA. Percentages were transformed using the classical arcsin transformation method to better-fit assumptions of normality and homogeneity of variance. Differences (diff) reported are from un-transformed data and reflect the mean difference in proportions of cells in the established firing rate bin, (i.e. -0.18 and -0.16, or 18% and 16% for SST-Lypd6 1d MD and SST-Lypd6 no MD respectively). Student's *t*-test was used for all other analyses that compare mean differences between two groups. A minimum *P* value of 0.05 was accepted as statistically significant. Other than LMM, all statistical analyses were performed using Prism 6.0h (GraphPad Software). All CBI, quantified expression, quantified co-localization, and visually evoked firing rate data in figures are presented as mean±SEM. No method of randomization was used to determine allocation of samples. No statistical methods were used to predetermine sample sizes. However, all cell and animal-level sample sizes for all experiments including quantified expression/co-localization experiments and *in vivo* extracellular electrophysiological experiments were selected based on previously published studies.

Data availability

The data that support the findings of this study are available from the corresponding author (H.M.) upon reasonable request.

Acknowledgments

This work was supported by National Eye Institute R01EY024918, R01EY 026053, R21EY026702 to H.M., National Institute on Drug Abuse T32 DA007135 to M.P.D., National Institute of Mental Health T32MH096678 to M.S., R21MH106919 to H.M., Knights Templar Eye Foundation to H.M., March of Dimes to H.M., Whitehall Foundation to H.M., and Brain and Behavior Research Foundation to H.M. AZ is a member of the Excellence Cluster Immunosensation. We thank Dr. Ming-Hu Han (Icahn School of Medicine at Mount Sinai) for providing technical expertise on optogenetics and Dr. Yasmin Hurd and Dr. Michael Michaelides (Icahn School of Medicine at Mount Sinai) for their expertise on chemogenetics.

Author Contributions

M.S., M.P.D., and H.M. designed research; M.S., M.P.D, P.N.B., P.Y., and H.M. performed research; A.Z. contributed unpublished reagents and provided expertise; M.S., M.P.D, P.N.B., P.Y., M.R.S., and H.M. analyzed data; M.S., M.P.D, and H.M. wrote the manuscript. The authors declare no conflicts of interest.

References

1 Hensch, T. K. Critical period regulation. *Annual review of neuroscience* **27**, 549-579, doi:10.1146/annurev.neuro.27.070203.144327 (2004).

2 Knudsen, E. I. Sensitive periods in the development of the brain and behavior. *Journal of cognitive neuroscience* **16**, 1412-1425, doi:10.1162/0898929042304796 (2004).

3 Wiesel, T. N. Postnatal development of the visual cortex and the influence of environment. *Nature* **299**, 583-591 (1982).

4 Espinosa, J. S. & Stryker, M. P. Development and plasticity of the primary visual cortex. *Neuron* **75**, 230-249, doi:10.1016/j.neuron.2012.06.009 (2012).

5 Morishita, H. & Hensch, T. K. Critical period revisited: impact on vision. *Current opinion in neurobiology* **18**, 101-107, doi:10.1016/j.conb.2008.05.009 (2008).

6 Hubener, M. & Bonhoeffer, T. Neuronal plasticity: beyond the critical period. *Cell* **159**, 727-737, doi:10.1016/j.cell.2014.10.035 (2014).

7 Levelt, C. N. & Hubener, M. Critical-period plasticity in the visual cortex. *Annual review of neuroscience* **35**, 309-330, doi:10.1146/annurev-neuro-061010-113813 (2012).

8 Deidda, G. *et al.* Early depolarizing GABA controls critical-period plasticity in the rat visual cortex. *Nature neuroscience* **18**, 87-96, doi:10.1038/nn.3890 (2015).

9 Huang, Z. J. *et al.* BDNF regulates the maturation of inhibition and the critical period of plasticity in mouse visual cortex. *Cell* **98**, 739-755 (1999).

10 Hanover, J. L., Huang, Z. J., Tonegawa, S. & Stryker, M. P. Brain-derived neurotrophic factor overexpression induces precocious critical period in mouse visual cortex. *The Journal of neuroscience : the official journal of the Society for Neuroscience* **19**, RC40 (1999).

11 Fagiolini, M. & Hensch, T. K. Inhibitory threshold for critical-period activation in primary visual cortex. *Nature* **404**, 183-186, doi:10.1038/35004582 (2000).

12 Chattopadhyaya, B. *et al.* GAD67-mediated GABA synthesis and signaling regulate inhibitory synaptic innervation in the visual cortex. *Neuron* **54**, 889-903, doi:10.1016/j.neuron.2007.05.015 (2007).

13 Iwai, Y., Fagiolini, M., Obata, K. & Hensch, T. K. Rapid critical period induction by tonic inhibition in visual cortex. *The Journal of neuroscience : the official journal of the Society for Neuroscience* **23**, 6695-6702 (2003).

14 Hensch, T. K. *et al.* Local GABA circuit control of experience-dependent plasticity in developing visual cortex. *Science* **282**, 1504-1508 (1998).

15 Sugiyama, S. *et al.* Experience-dependent transfer of Otx2 homeoprotein into the visual cortex activates postnatal plasticity. *Cell* **134**, 508-520, doi:10.1016/j.cell.2008.05.054 (2008).

16 Hensch, T. K. Critical period plasticity in local cortical circuits. *Nature reviews. Neuroscience* **6**, 877-888, doi:10.1038/nrn1787 (2005).

17 Harauzov, A. *et al.* Reducing intracortical inhibition in the adult visual cortex promotes ocular dominance plasticity. *The Journal of neuroscience : the official journal of the Society for Neuroscience* **30**, 361-371, doi:10.1523/JNEUROSCI.2233-09.2010 (2010).

18 Southwell, D. G., Froemke, R. C., Alvarez-Buylla, A., Stryker, M. P. & Gandhi, S. P. Cortical plasticity induced by inhibitory neuron transplantation. *Science* **327**, 1145-1148, doi:10.1126/science.1183962 (2010).

19 Tang, Y., Stryker, M. P., Alvarez-Buylla, A. & Espinosa, J. S. Cortical plasticity induced by transplantation of embryonic somatostatin or parvalbumin interneurons. *Proceedings of the National Academy of Sciences of the United States of America* **111**, 18339-18344, doi:10.1073/pnas.1421844112 (2014).

20 Davis, M. F. *et al.* Inhibitory Neuron Transplantation into Adult Visual Cortex Creates a New Critical Period that Rescues Impaired Vision. *Neuron* **86**, 1055-1066, doi:10.1016/j.neuron.2015.03.062 (2015).

21 Yazaki-Sugiyama, Y., Kang, S., Cateau, H., Fukai, T. & Hensch, T. K. Bidirectional plasticity in fast-spiking GABA circuits by visual experience. *Nature* **462**, 218-221, doi:10.1038/nature08485 (2009).

22 Kuhlman, S. J. *et al.* A disinhibitory microcircuit initiates critical-period plasticity in the visual cortex. *Nature* **501**, 543-546, doi:10.1038/nature12485 (2013).

23 Pizzorusso, T. *et al.* Reactivation of ocular dominance plasticity in the adult visual cortex. *Science* **298**, 1248-1251, doi:10.1126/science.1072699 (2002).

24 Beurdeley, M. *et al.* Otx2 binding to perineuronal nets persistently regulates plasticity in the mature visual cortex. *The Journal of neuroscience : the official journal of the Society for Neuroscience* **32**, 9429-9437, doi:10.1523/JNEUROSCI.0394-12.2012 (2012).

25 Rudy, B., Fishell, G., Lee, S. & Hjerling-Leffler, J. Three groups of interneurons account for nearly 100% of neocortical GABAergic neurons. *Developmental neurobiology* **71**, 45-61, doi:10.1002/dneu.20853 (2011).

26 Fu, Y., Kaneko, M., Tang, Y., Alvarez-Buylla, A. & Stryker, M. P. A cortical disinhibitory circuit for enhancing adult plasticity. *eLife* **4**, e05558, doi:10.7554/eLife.05558 (2015).

27 Tan, Z., Hu, H., Huang, Z. J. & Agmon, A. Robust but delayed thalamocortical activation of dendritic-targeting inhibitory interneurons. *Proceedings of the National Academy of Sciences of the United States of America* **105**, 2187-2192, doi:10.1073/pnas.0710628105 (2008).

28 Chen, N., Sugihara, H. & Sur, M. An acetylcholine-activated microcircuit drives temporal dynamics of cortical activity. *Nature neuroscience* **18**, 892-902, doi:10.1038/nn.4002 (2015).

29 Pakan, J. M. *et al.* Behavioral-state modulation of inhibition is context-dependent and cell type specific in mouse visual cortex. *eLife* **5**, doi:10.7554/eLife.14985 (2016).

30 Dipoppa, M. *et al.* Vision and locomotion shape the interactions between neuron types in mouse visual cortex. *bioRxiv*, doi:10.1101/058396 (2016).

31 Polack, P. O., Friedman, J. & Golshani, P. Cellular mechanisms of brain state-dependent gain modulation in visual cortex. *Nature neuroscience* **16**, 1331-1339, doi:10.1038/nn.3464 (2013).

32 Fu, Y. *et al.* A cortical circuit for gain control by behavioral state. *Cell* **156**, 1139-1152, doi:10.1016/j.cell.2014.01.050 (2014).

33 Reimer, J. *et al.* Pupil fluctuations track fast switching of cortical states during quiet wakefulness. *Neuron* **84**, 355-362, doi:10.1016/j.neuron.2014.09.033 (2014).

34 Zhang, S. *et al.* Selective attention. Long-range and local circuits for top-down modulation of visual cortex processing. *Science* **345**, 660-665, doi:10.1126/science.1254126 (2014).

35 Lee, S., Kruglikov, I., Huang, Z. J., Fishell, G. & Rudy, B. A disinhibitory circuit mediates motor integration in the somatosensory cortex. *Nature neuroscience* **16**, 1662-1670, doi:10.1038/nn.3544 (2013).

36 Makino, H. & Komiyama, T. Learning enhances the relative impact of top-down processing in the visual cortex. *Nature neuroscience* **18**, 1116-1122, doi:10.1038/nn.4061 (2015).

37 Zhao-Shea, R., Liu, L., Pang, X., Gardner, P. D. & Tapper, A. R. Activation of GABAergic neurons in the interpeduncular nucleus triggers physical nicotine withdrawal symptoms. *Current biology : CB* **23**, 2327-2335, doi:10.1016/j.cub.2013.09.041 (2013).

38 Leao, R. N. *et al.* OLM interneurons differentially modulate CA3 and entorhinal inputs to hippocampal CA1 neurons. *Nature neuroscience* **15**, 1524-1530, doi:10.1038/nn.3235 (2012).

39 Jia, Y., Yamazaki, Y., Nakauchi, S., Ito, K. & Sumikawa, K. Nicotine facilitates long-term potentiation induction in oriens-lacunosum moleculare cells via Ca2+ entry through non-alpha7 nicotinic acetylcholine receptors. *The European journal of neuroscience* **31**, 463-476, doi:10.1111/j.1460-9568.2009.07058.x (2010).

40 Morishita, H., Miwa, J. M., Heintz, N. & Hensch, T. K. Lynx1, a cholinergic brake, limits plasticity in adult visual cortex. *Science* **330**, 1238-1240, doi:10.1126/science.1195320 (2010).

41 Miwa, J. M., Lester, H. A. & Walz, A. Optimizing cholinergic tone through lynx modulators of nicotinic receptors: implications for plasticity and nicotine addiction. *Physiology (Bethesda)* **27**, 187-199, doi:10.1152/physiol.00002.2012 (2012).

42 Demars, M. P. & Morishita, H. Cortical parvalbumin and somatostatin GABA neurons express distinct endogenous modulators of nicotinic acetylcholine receptors. *Molecular brain* **7**, 75, doi:10.1186/s13041-014-0075-9 (2014).

43 Darvas, M. *et al.* Modulation of the Ca2+ conductance of nicotinic acetylcholine receptors by Lypd6. *European neuropsychopharmacology : the journal of the European College of Neuropsychopharmacology* **19**, 670-681, doi:10.1016/j.euroneuro.2009.03.007 (2009).

44 Miwa, J. M. *et al.* The prototoxin lynx1 acts on nicotinic acetylcholine receptors to balance neuronal activity and survival in vivo. *Neuron* **51**, 587-600, doi:10.1016/j.neuron.2006.07.025 (2006).

45 Sadahiro, M., Sajo, M. & Morishita, H. Nicotinic regulation of experience-dependent plasticity in visual cortex. *Journal of physiology, Paris* **110**, 29-36, doi:10.1016/j.jphysparis.2016.11.003 (2016).

46 Bukhari, N. *et al.* Unmasking Proteolytic Activity for Adult Visual Cortex Plasticity by the Removal of Lynx1. *The Journal of neuroscience : the official journal of the Society for Neuroscience* **35**, 12693-12702, doi:10.1523/JNEUROSCI.4315-14.2015 (2015).

47 Koike, H. *et al.* Chemogenetic Inactivation of Dorsal Anterior Cingulate Cortex Neurons Disrupts Attentional Behavior in Mouse. *Neuropsychopharmacology : official publication of the American College of Neuropsychopharmacology* **41**, 1014-1023, doi:10.1038/npp.2015.229 (2016).

48 Heys, J. G., Schultheiss, N. W., Shay, C. F., Tsuno, Y. & Hasselmo, M. E. Effects of acetylcholine on neuronal properties in entorhinal cortex. *Frontiers in behavioral neuroscience* **6**, 32, doi:10.3389/fnbeh.2012.00032 (2012).

49 Ishii, K., Wong, J. K. & Sumikawa, K. Comparison of alpha2 nicotinic acetylcholine receptor subunit mRNA expression in the central nervous system of rats and mice. *The Journal of comparative neurology* **493**, 241-260, doi:10.1002/cne.20762 (2005).

50 Tasic, B. *et al.* Adult mouse cortical cell taxonomy revealed by single cell transcriptomics. *Nature neuroscience* **19**, 335-346, doi:10.1038/nn.4216 (2016).

51 Lotfipour, S. *et al.* Targeted deletion of the mouse alpha2 nicotinic acetylcholine receptor subunit gene (Chrna2) potentiates nicotine-modulated behaviors. *The Journal of neuroscience : the official journal of the Society for Neuroscience* **33**, 7728-7741, doi:10.1523/JNEUROSCI.4731-12.2013 (2013).

52 Kalogeraki, E., Greifzu, F., Haack, F. & Lowel, S. Voluntary physical exercise promotes ocular dominance plasticity in adult mouse primary visual cortex. *The Journal of neuroscience : the official journal of the Society for Neuroscience* **34**, 15476-15481, doi:10.1523/JNEUROSCI.2678-14.2014 (2014).

53 Hioki, H. *et al.* Cell type-specific inhibitory inputs to dendritic and somatic compartments of parvalbumin-expressing neocortical interneuron. *The Journal of neuroscience : the official journal of the Society for Neuroscience* **33**, 544-555, doi:10.1523/JNEUROSCI.2255-12.2013 (2013).

54 Pfeffer, C. K., Xue, M., He, M., Huang, Z. J. & Scanziani, M. Inhibition of inhibition in visual cortex: the logic of connections between molecularly distinct interneurons. *Nature neuroscience* **16**, 1068-1076, doi:10.1038/nn.3446 (2013).

55 Xu, H., Jeong, H. Y., Tremblay, R. & Rudy, B. Neocortical somatostatin-expressing GABAergic interneurons disinhibit the thalamorecipient layer 4. *Neuron* **77**, 155-167, doi:10.1016/j.neuron.2012.11.004 (2013).

56 Sturgill, J. F. & Isaacson, J. S. Somatostatin cells regulate sensory response fidelity via subtractive inhibition in olfactory cortex. *Nature neuroscience* **18**, 531-535, doi:10.1038/nn.3971 (2015).

57 Hu, H., Ma, Y. & Agmon, A. Submillisecond firing synchrony between different subtypes of cortical interneurons connected chemically but not electrically. *The Journal of neuroscience : the official journal of the Society for Neuroscience* **31**, 3351-3361, doi:10.1523/JNEUROSCI.4881-10.2011 (2011).

58 Cottam, J. C., Smith, S. L. & Hausser, M. Target-specific effects of somatostatin-expressing interneurons on neocortical visual processing. *The Journal of neuroscience : the official journal of the Society for Neuroscience* **33**, 19567-19578, doi:10.1523/JNEUROSCI.2624-13.2013 (2013).

59 Urban, D. J. & Roth, B. L. DREADDs (designer receptors exclusively activated by designer drugs): chemogenetic tools with therapeutic utility. *Annual review of pharmacology and toxicology* **55**, 399-417, doi:10.1146/annurev-pharmtox-010814-124803 (2015).

60 Ozhan, G. *et al.* Lypd6 enhances Wnt/beta-catenin signaling by promoting Lrp6 phosphorylation in raft plasma membrane domains. *Developmental cell* **26**, 331-345, doi:10.1016/j.devcel.2013.07.020 (2013).

61 Thomsen, M. S. *et al.* Expression of the Ly-6 family proteins Lynx1 and Ly6H in the rat brain is compartmentalized, cell-type specific, and developmentally regulated. *Brain structure & function* **219**, 1923-1934, doi:10.1007/s00429-013-0611-x (2014).

62 Arvaniti, M. *et al.* Functional interaction between Lypd6 and nicotinic acetylcholine receptors. *Journal of neurochemistry* **138**, 806-820, doi:10.1111/jnc.13718 (2016).

63 Marchi, M. & Grilli, M. Presynaptic nicotinic receptors modulating neurotransmitter release in the central nervous system: functional interactions with other coexisting receptors. *Progress in neurobiology* **92**, 105-111, doi:10.1016/j.pneurobio.2010.06.004 (2010).

64 Mikuni, T., Nishiyama, J., Sun, Y., Kamasawa, N. & Yasuda, R. High-Throughput, High-Resolution Mapping of Protein Localization in Mammalian Brain by In Vivo Genome Editing. *Cell* **165**, 1803-1817, doi:10.1016/j.cell.2016.04.044 (2016).

65 Poorthuis, R. B., Bloem, B., Verhoog, M. B. & Mansvelder, H. D. Layer-specific interference with cholinergic signaling in the prefrontal cortex by smoking concentrations of nicotine. *The Journal of neuroscience : the official journal of the Society for Neuroscience* **33**, 4843-4853, doi:10.1523/JNEUROSCI.5012-12.2013 (2013).

66 Gulledge, A. T., Park, S. B., Kawaguchi, Y. & Stuart, G. J. Heterogeneity of phasic cholinergic signaling in neocortical neurons. *Journal of neurophysiology* **97**, 2215-2229, doi:10.1152/jn.00493.2006 (2007).

67 Porter, J. T. *et al.* Selective excitation of subtypes of neocortical interneurons by nicotinic receptors. *The Journal of neuroscience : the official journal of the Society for Neuroscience* **19**, 5228-5235 (1999).

68 Alitto, H. J. & Dan, Y. Cell-type-specific modulation of neocortical activity by basal forebrain input. *Frontiers in systems neuroscience* **6**, 79, doi:10.3389/fnsys.2012.00079 (2012).

69 Jiang, X. *et al.* Principles of connectivity among morphologically defined cell types in adult neocortex. *Science* **350**, aac9462, doi:10.1126/science.aac9462 (2015).

70 Gerfen, C. R., Paletzki, R. & Heintz, N. GENSAT BAC cre-recombinase driver lines to study the functional organization of cerebral cortical and basal ganglia circuits. *Neuron* **80**, 1368-1383, doi:10.1016/j.neuron.2013.10.016 (2013).

71 Kolisnyk, B. *et al.* ChAT-ChR2-EYFP mice have enhanced motor endurance but show deficits in attention and several additional cognitive domains. *The Journal of neuroscience : the official journal of the Society for Neuroscience* **33**, 10427-10438, doi:10.1523/JNEUROSCI.0395-13.2013 (2013).

72 Nakauchi, S., Brennan, R. J., Boulter, J. & Sumikawa, K. Nicotine gates long-term potentiation in the hippocampal CA1 region via the activation of alpha2* nicotinic ACh receptors. *The European journal of neuroscience* **25**, 2666-2681, doi:10.1111/j.1460-9568.2007.05513.x (2007).

73 van Versendaal, D. *et al.* Elimination of inhibitory synapses is a major component of adult ocular dominance plasticity. *Neuron* **74**, 374-383, doi:10.1016/j.neuron.2012.03.015 (2012).

74 Chen, J. L. *et al.* Clustered dynamics of inhibitory synapses and dendritic spines in the adult neocortex. *Neuron* **74**, 361-373, doi:10.1016/j.neuron.2012.02.030 (2012).

75 Lazarus, M. S. & Huang, Z. J. Distinct maturation profiles of perisomatic and dendritic targeting GABAergic interneurons in the mouse primary visual cortex during the critical period of ocular dominance plasticity. *Journal of neurophysiology* **106**, 775-787, doi:10.1152/jn.00729.2010 (2011).

76 Wang, J. *et al.* An Accessory Agonist Binding Site Promotes Activation of alpha4beta2* Nicotinic Acetylcholine Receptors. *The Journal of biological chemistry* **290**, 13907-13918, doi:10.1074/jbc.M115.646786 (2015).

77 Wang, J. *et al.* A Novel alpha2/alpha4 Subtype-selective Positive Allosteric Modulator of Nicotinic Acetylcholine Receptors Acting from the C-tail of an alpha Subunit. *The Journal of biological chemistry* **290**, 28834-28846, doi:10.1074/jbc.M115.676551 (2015).

78 Timmermann, D. B. *et al.* Augmentation of cognitive function by NS9283, a stoichiometry-dependent positive allosteric modulator of alpha2- and alpha4-containing nicotinic acetylcholine receptors. *British journal of pharmacology* **167**, 164-182, doi:10.1111/j.1476-5381.2012.01989.x (2012).

79 Reimers, K., Emmert, N., Shah, H., Benedict, R. H. & Szigeti, K. Capgras-like visual decomposition in Lewy body dementia with therapeutic response to donepezil. *Neurology. Clinical practice* **4**, 467-469, doi:10.1212/CPJ.0000000000000068 (2014).

80 Klassen, T. *et al.* Exome sequencing of ion channel genes reveals complex profiles confounding personal risk assessment in epilepsy. *Cell* **145**, 1036-1048, doi:10.1016/j.cell.2011.05.025 (2011).

81 Conti, V. *et al.* Nocturnal frontal lobe epilepsy with paroxysmal arousals due to CHRNA2 loss of function. *Neurology* **84**, 1520-1528, doi:10.1212/WNL.0000000000001471 (2015).

82 Yang, J. *et al.* The contribution of rare and common variants in 30 genes to risk nicotine dependence. *Molecular psychiatry*, doi:10.1038/mp.2014.156 (2014).

83 Won, H. *et al.* Chromosome conformation elucidates regulatory relationships in developing human brain. *Nature* **538**, 523-527, doi:10.1038/nature19847 (2016).

84 Tai, C., Abe, Y., Westenbroek, R. E., Scheuer, T. & Catterall, W. A. Impaired excitability of somatostatin- and parvalbumin-expressing cortical interneurons in a mouse model of Dravet syndrome. *Proceedings of the National Academy of Sciences of the United States of America* **111**, E3139-3148, doi:10.1073/pnas.1411131111 (2014).

85 Paluszkiewicz, S. M., Olmos-Serrano, J. L., Corbin, J. G. & Huntsman, M. M. Impaired inhibitory control of cortical synchronization in fragile X syndrome. *Journal of neurophysiology* **106**, 2264-2272, doi:10.1152/jn.00421.2011 (2011).

86 Hashimoto, T. *et al.* Conserved regional patterns of GABA-related transcript expression in the neocortex of subjects with schizophrenia. *The American journal of psychiatry* **165**, 479-489, doi:10.1176/appi.ajp.2007.07081223 (2008).

87 Fung, S. J. *et al.* Expression of interneuron markers in the dorsolateral prefrontal cortex of the developing human and in schizophrenia. *The American journal of psychiatry* **167**, 1479-1488, doi:10.1176/appi.ajp.2010.09060784 (2010).

88 Lin, L. C. & Sibille, E. Reduced brain somatostatin in mood disorders: a common pathophysiological substrate and drug target? *Frontiers in pharmacology* **4**, 110, doi:10.3389/fphar.2013.00110 (2013).

89 Zhang, W. *et al.* Hyperactive somatostatin interneurons contribute to excitotoxicity in neurodegenerative disorders. *Nature neuroscience* **19**, 557-559, doi:10.1038/nn.4257 (2016).

90 Schmid, L. C. *et al.* Dysfunction of Somatostatin-Positive Interneurons Associated with Memory Deficits in an Alzheimer's Disease Model. *Neuron* **92**, 114-125, doi:10.1016/j.neuron.2016.08.034 (2016).

Figure Legends

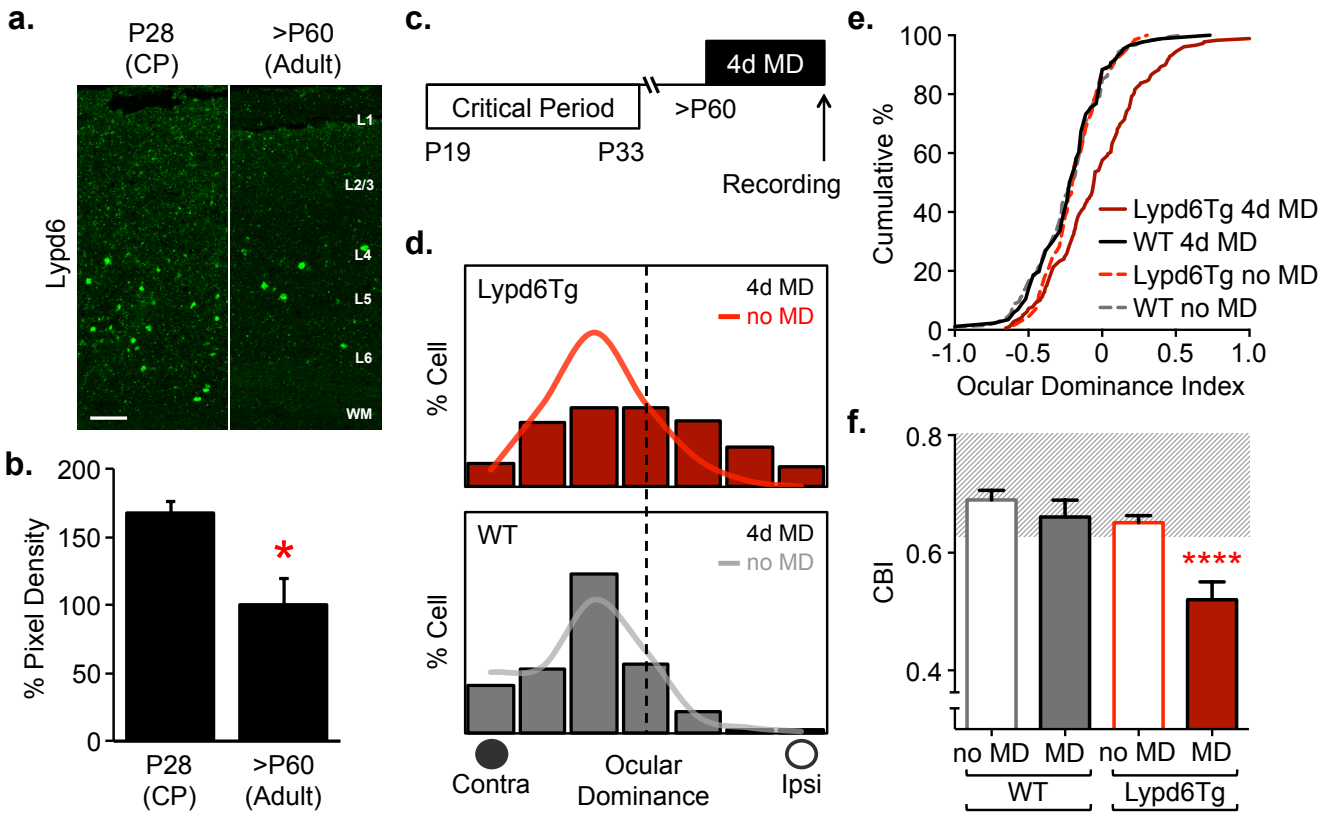

Figure 1 | Neuronal overexpression of Lypd6 prolongs ocular dominance plasticity into adulthood. (a) Representative images of fluorescent *in situ* hybridization labeling of *Lypd6* mRNA in V1 binocular zone from critical period (CP: P28) and adult (>P60) mice. Scale bar=100μm. **(b)** Quantification of Lypd6 *mRNA* expression in V1 of P28 and >P60 mice. Lypd6 level is higher in CP mice in comparison to Adult mice [CP: P28, n=4 mice; Adult: >P60, n=3 mice]: **P*=0.02, Student's *t*-test. Data in figure presented as mean±SEM. **(c)** Schematic representation of V1 plasticity paradigm by 4 days of monocular deprivation (4d MD) in adult Lypd6Tg or WT mice. **(d)** Adult 4d MD results in a shift in ocular dominance distribution of Lypd6Tg mice [red bar histogram; n=179 cells from 9 mice] but not in WT mice [gray bar histogram; n=86 cells from 7 mice]: *****P*<0.0001. Lypd6Tg 4d MD vs. Lypd6Tg no MD [red line histogram; n=67 cells from 4 mice]: *****P*<0.0001. Lypd6Tg no MD vs. WT no MD [gray line histogram; n=193 cells from 11 mice]: *P*=0.28, χ^2 test. χ^2 tests were conducted based on

actual cell numbers recorded. Histograms from groups for main comparisons are presented in bar format. Other control groups are overlaid in line format. Histograms are presented in percentage of cells representing each ocular dominance score. Filled circle labeled as “contra” represents contralateral eye that received monocular deprivation in MD designated groups, whereas empty circle labeled as “ipsi” represents the ipsilateral non-deprived eye. **(e)** Cumulative plot of quantified spike response of each unit (ocular dominance index) after adult 4d MD confirms ocular dominance shift in Lypd6Tg mice [red line; n=179 cells from 9 mice] but not in WT mice [black line; n=86 cells from 7 mice]: ****P<0.0001. Lypd6Tg 4d MD vs. Lypd6Tg no MD [dashed bright red line; n=67 cells from 4 mice]: ***P=0.0002. Lypd6Tg no MD vs. WT no MD [dashed gray line; n=193 cells from 11 mice]: P=0.2332, Kolmogorov-Smirnov (K-S) test. **(f)** Comparison of contralateral bias index (CBI) following adult 4d MD in WT mice [gray solid bar; CBI=0.66, n=7 mice] and Lypd6Tg mice [red solid bar; CBI=0.52, n=9 mice], or no MD in WT mice [gray open bar; CBI=0.66, n=11 mice] and Lypd6Tg mice [red open bar; CBI=0.65, n=4 mice]: ****P<0.0001, one-way analysis of variance (ANOVA). Lypd6Tg 4d MD significantly differs from all other groups: WT no MD, WT4d MD, and Lypd6Tg no MD: respectively, ****P<0.0001, **P=0.0023, and *P=0.0208; Tukey’s multiple comparisons test. Gray background area represents CBI range in a non-plastic mouse. Data in figure presented as ±SEM.

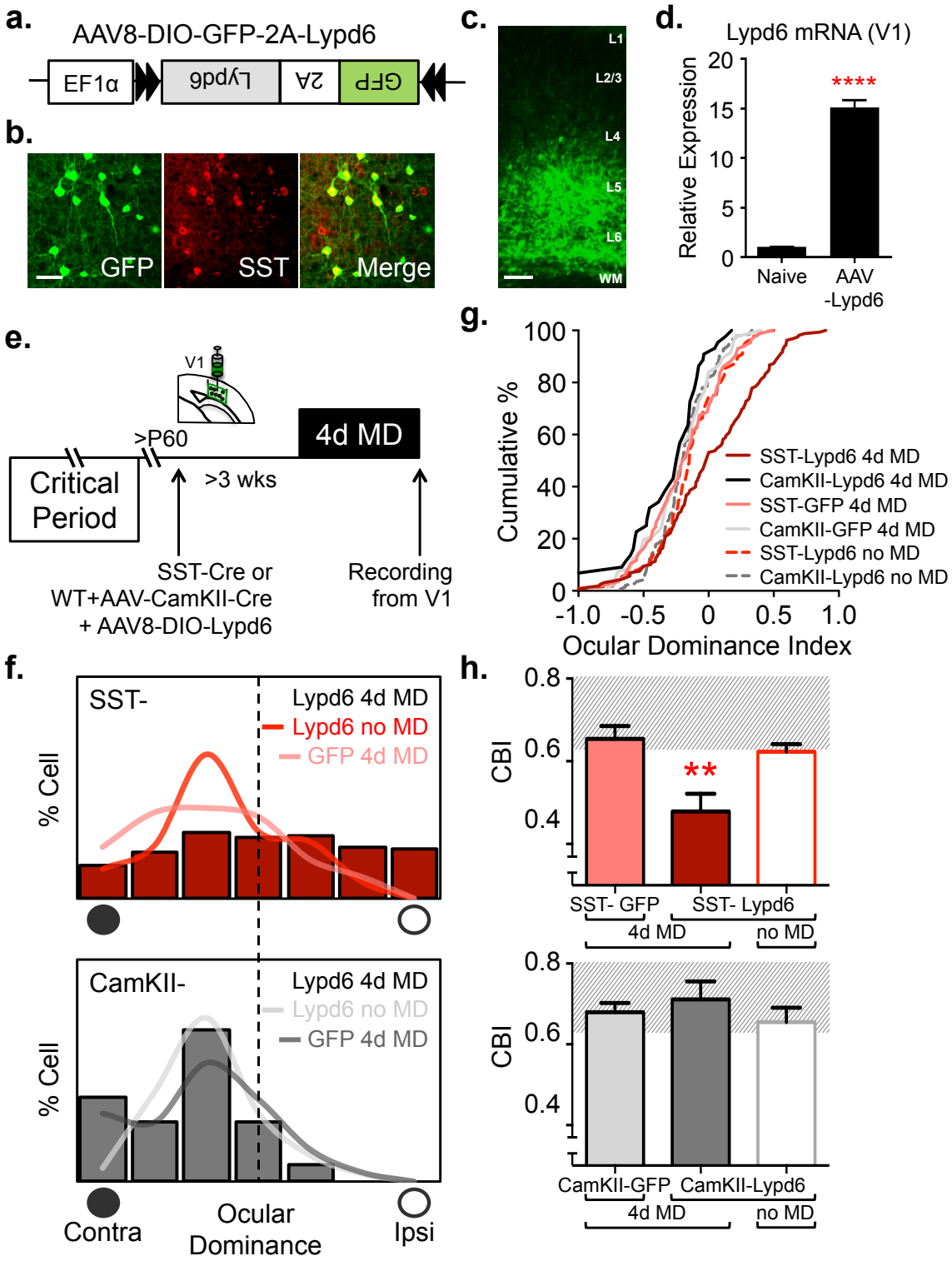

Figure 2 | Selective overexpression of Lypd6 specifically in SST interneurons reactivates ocular dominance plasticity in adult V1. (a) Schematic representation of adeno-associated viral (AAV)

construct for cre-dependent Lypd6 over-expression. Bicistronic expression of GFP and Lypd6 is achieved through the use of a 2A sequence. **(b)** Representative images of viral GFP labeling following injection of AAV8-DIO-GFP-2A-Lypd6 (AAV-Lypd6) into V1 of SST-cre mice. Immunohistochemical labeling shows specific expression of GFP (green) overlapping immunolabeled SST (red) neurons. 98±1.52% of GFP labeled cells co-labeled with SST [n=2 mice]. Data is mean±SEM. Scale bar=50μm. **(c)** Representative image of V1 layers following injection of AAV-Lypd6 targeting the deep layers in SST-Cre mice. Viral transduction represented by GFP (green) labeling is concentrated in layers V and VI. Scale bar=100μm. **(d)** Quantitative PCR of *Lypd6* mRNA from cDNA derived from whole V1 extracts of naïve and AAV-Lypd6 injected SST-cre mice [ΔΔCT method, n=3 mice]: ****P<0.0001, Student's t-test. Data in figure presented as mean±SEM. **(e)** Schematic representation of V1 plasticity paradigm by 4d MD with viral injection. AAV-Lypd6 was injected into binocular zone of V1 of adult (>P60) SST-cre mice (SST-Lypd6), or as a cocktail with AAV-CamKII-cre in adult WT mice (CamKII-Lypd6) and incubated for >3 weeks prior to 4d MD. **(f)** Adult 4d MD results in a shift in ocular dominance distribution of SST-Lypd6 mice [red bar histogram; n=158 cells from 9 mice] but not in WT mice injected with a cocktail of AAV-CamKII-cre and AAV-Lypd6 (CamKII-Lypd6) [gray bar histogram; n=44 cells from 3 mice]: ****P<0.0001. SST-Lypd6 4d MD: vs. SST-Lypd6 no MD [red line histogram; n=110 cells from 5 mice]: ****P<0.0001, vs. SST-GFP 4d MD [pink line histogram; n=86 cells from 5 mice]: ***P=0.0006. CamKII-Lypd6 4d MD vs. CamKII-GFP 4d MD [gray line histogram; n=81 cells from 4 mice]: P=0.67, χ^2 test. **(g)** Cumulative plot of ocular dominance index after adult 4d MD confirms ocular dominance shift in SST-Lypd6 mice [red line; n=158 cells from 9 mice] but not in CamKII-Lypd6 mice [black line; n=44 cells from 3 mice]: ****P<0.0001. SST-Lypd6 4d MD: vs. SST-Lypd6 no MD [dashed bright red line; n=110 cells from 5 mice]: ***P=0.0001, vs. SST-GFP 4d MD [pink line; n=86 cells from 5 mice]: ***P=0.0002. CamKII-Lypd6 4d MD vs. CamKII-GFP 4d MD [light gray line; n=81 cells from 4 mice]: P=0.49, K-S test. **(h)** Comparison of contralateral bias index (CBI) following adult 4d MD in SST-GFP [pink solid bar; CBI=0.65, n=5 mice], SST-Lypd6 [red solid bar; CBI=0.48, n=9 mice], CamKII-GFP [light gray solid bar; CBI=0.68, n=4 mice] and CamKII-Lypd6 mice [dark gray solid bar; CBI=0.71, n=3

mice] with non-deprived SST-Lypd6 [red open bar; CBI=0.62, n=5 mice] and non-deprived CamKII-Lypd6 [gray open bar; CBI=0.66, n=5 mice]: ***P*=0.0014, one-way ANOVA. SST-Lypd6 4d MD significantly differs from: SST-Lypd6 no MD, SST-GFP 4d MD, and CamKII-Lypd6 4d MD: respectively, ***P*=0.0477, ***P*=0.0183, and ****P*=0.0073. CamKII-Lypd6 4d MD does not differ from CamKII-Lypd6 no MD or CamKII-GFP 4d MD: respectively, *P*=0.9527, and *P*=0.9969; Tukey's multiple comparisons test. Gray background area represents CBI range in a non-plastic mouse. Data in figure presented as mean±SEM.

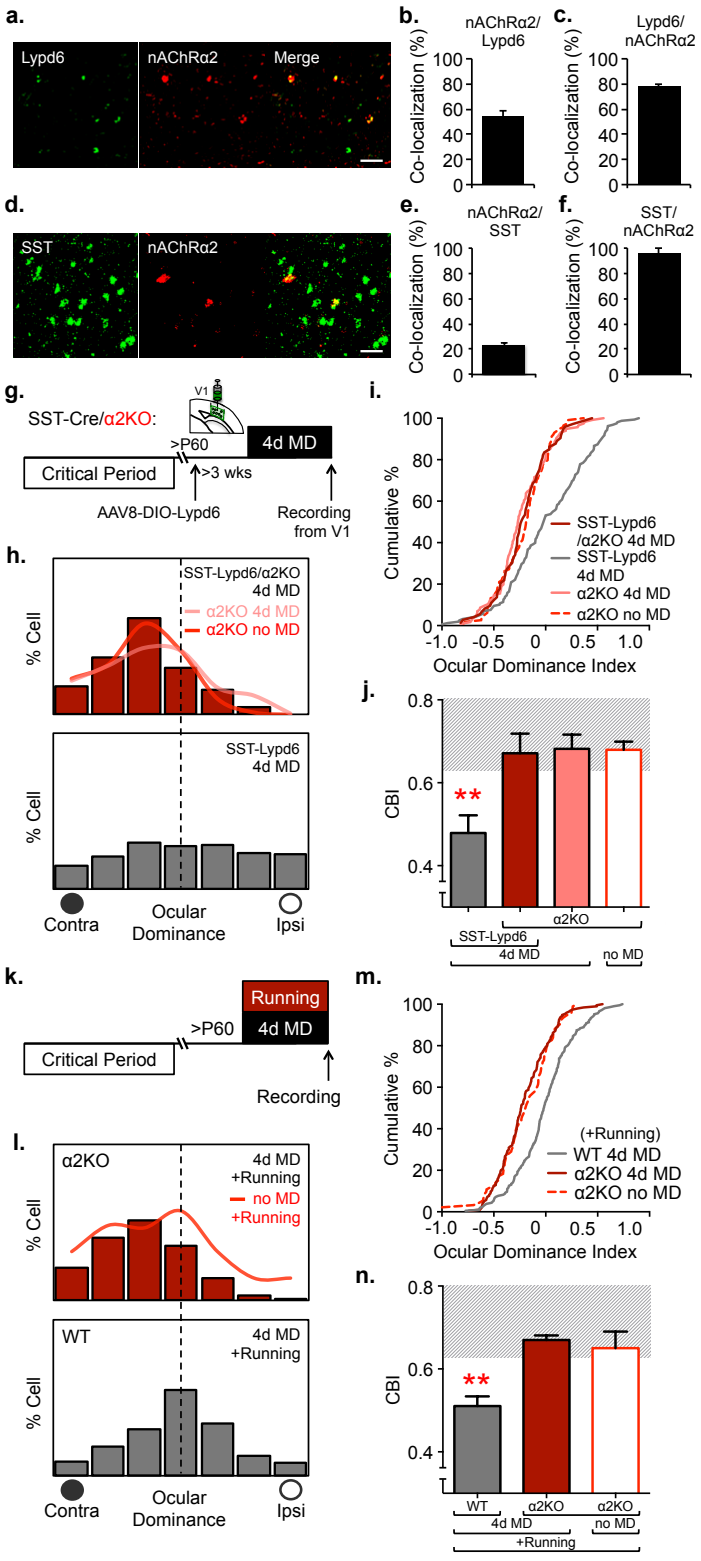

Figure 3 | α2 nicotinic acetylcholine receptor subunit is required for reactivation of ocular dominance plasticity in adulthood. (a) Representative images of double fluorescent labeling of

mRNA in V1 for *Lypd6* (green) and *α2 nicotinic acetylcholine receptor (Chrna2: nAChRα2)* (red). Scale bar=50μm. **(b)** 53±3.26% of *Lypd6* mRNA labeled cells co-express *nAChRα2* mRNA. [n=2 mice]. **(c)** 79±2.93% of *nAChRα2* mRNA labeled cell co-express *Lypd6* mRNA. [n=2 mice]. Data in **b** and **c** are presented as mean±SEM. **(d)** Representative images of double fluorescent *in situ* hybridization labeling of mRNA in V1 for *SST* (green) and *nAChRα2* (red). Scale bar=50μm. **(e)** 23±0.01% of *SST* mRNA labeled cell co-express *nAChRα2* mRNA. [n= 2 mice]. **(f)** 95±0.04% of *nAChRα2* mRNA labeled cells co-express *SST* mRNA. [n=2 mice]. Data in **e** and **f** are presented as mean±SEM. **(g)** Schematic representation of experiment for **h-j**: V1 plasticity paradigm by 4d MD with viral injection. AAV-Lypd6 was injected into V1 binocular zone of adult (>P60) bigenic SST-cre/Chrna2KO mice (SST-Lypd6/α2KO), or adult SST-cre mice (SST-Lypd6) and incubated for >3 weeks prior to 4d MD. **(h)** Adult 4d MD results in a significantly decreased shift in ocular dominance distribution of bigenic SST-Lypd6/α2KO mice [red bar histogram; n=73 cells from 5 mice] when compared with ocular dominance shift in adult 4d MD SST-Lypd6 mice [gray bar histogram; data in Fig. 2e legend]: ****P<0.0001. SST-Lypd6/α2KO 4d MD vs. α2KO 4d MD [pink line histogram; n=116 cells from 3 mice]: P=0.62. α2KO 4d MD vs. α2KO no MD [red line histogram; n=114 cells from 4 mice]: P=0.24, χ^2 test. **(i)** Cumulative plot of ocular dominance index after adult 4d MD confirms significant ablation of ocular dominance shift in absence of nAChRα2 in deprived SST-Lypd6/α2KO mice [red line; n=73 cells from 5 mice] compared with SST-Lypd6 mice [gray line; data in Fig. 2f legend]: ****P<0.0001. SST-Lypd6/α2KO 4d MD vs. α2KO 4d MD [pink line; n=116 cells from 3 mice]: P=0.64. α2KO 4d MD vs. α2KO no MD [dashed bright red line; n=114 cells from 4 mice]: P=0.06, K-S test. **(j)** Comparison of contralateral bias index (CBI) following adult 4d MD in SST-Lypd6 mice [gray solid bar; data in Fig. 2g legend], SST-Lypd6/α2KO mice [red solid bar; CBI=0.66, n=5 mice], and α2KO mice [pink solid bar; CBI=0.68, n=3 mice], or no MD in α2KO mice [bright red open bar; CBI=0.68, n=4 mice]: **P=0.0053, one-way ANOVA. SST-Lypd6/α2KO 4d MD is only significantly different with SST-Lypd6 4d MD: *P=0.0209, and is not different from α2KO 4d MD: P=0.9990. α2KO 4d MD vs. α2KO no MD: P>0.9999; Tukey's multiple comparisons test. Gray background area represents CBI range in a non-plastic mouse. Data in figure

presented as mean±SEM. **(k)** Schematic representation of experiment for **l-n**; V1 plasticity paradigm by 4d MD with simultaneous 4 days of voluntary physical exercise through the use of a running wheel (Running) in single housed adult α2KO and WT mice. **(l)** Adult 4d MD with simultaneous Running results in a shift in ocular dominance distribution of WT mice [gray bar histogram; n=207 cells from 5 mice] but not in α2KO mice [red bar histogram; n=194 cells from 4 mice]: ****P<0.0001, χ^2 test. α2KO 4d MD +Running vs α2KO no MD+ Running [red line histogram; n=93 cells from 4 mice]: P=0.35, χ^2 test. **(m)** Cumulative plot of ocular dominance index after adult 4d MD with simultaneous Running confirms ocular dominance shift in WT mice [gray line; n=207 cells from 5 mice] but not in α2KO mice [red line; n=194 cells from 4 mice]: ****P<0.0001. Additionally, α2KO 4d MD+Running vs. α2KO no MD+Running [dashed bright red line; n=93 cells from 4 mice]: P=0.33, K-S test. **(n)** Comparison of contralateral bias index (CBI) following adult 4d MD with simultaneous Running in WT mice [gray solid bar; CBI=0.51, n=5 mice] and α2KO mice [red solid bar; CBI=0.67, n=4 mice], or no MD with simultaneous Running in α2KO mice [red open bar; CBI=0.65, n=4 mice]: **P=0.0030, one-way ANOVA. α2KO 4d MD+Running vs WT 4d MD+Running: **P=0.0046, vs α2KO no MD+Running: **P=0.0103; Tukey's multiple comparisons test. Gray background area represents CBI range in a non-plastic mouse. Data in figure presented as mean±SEM.

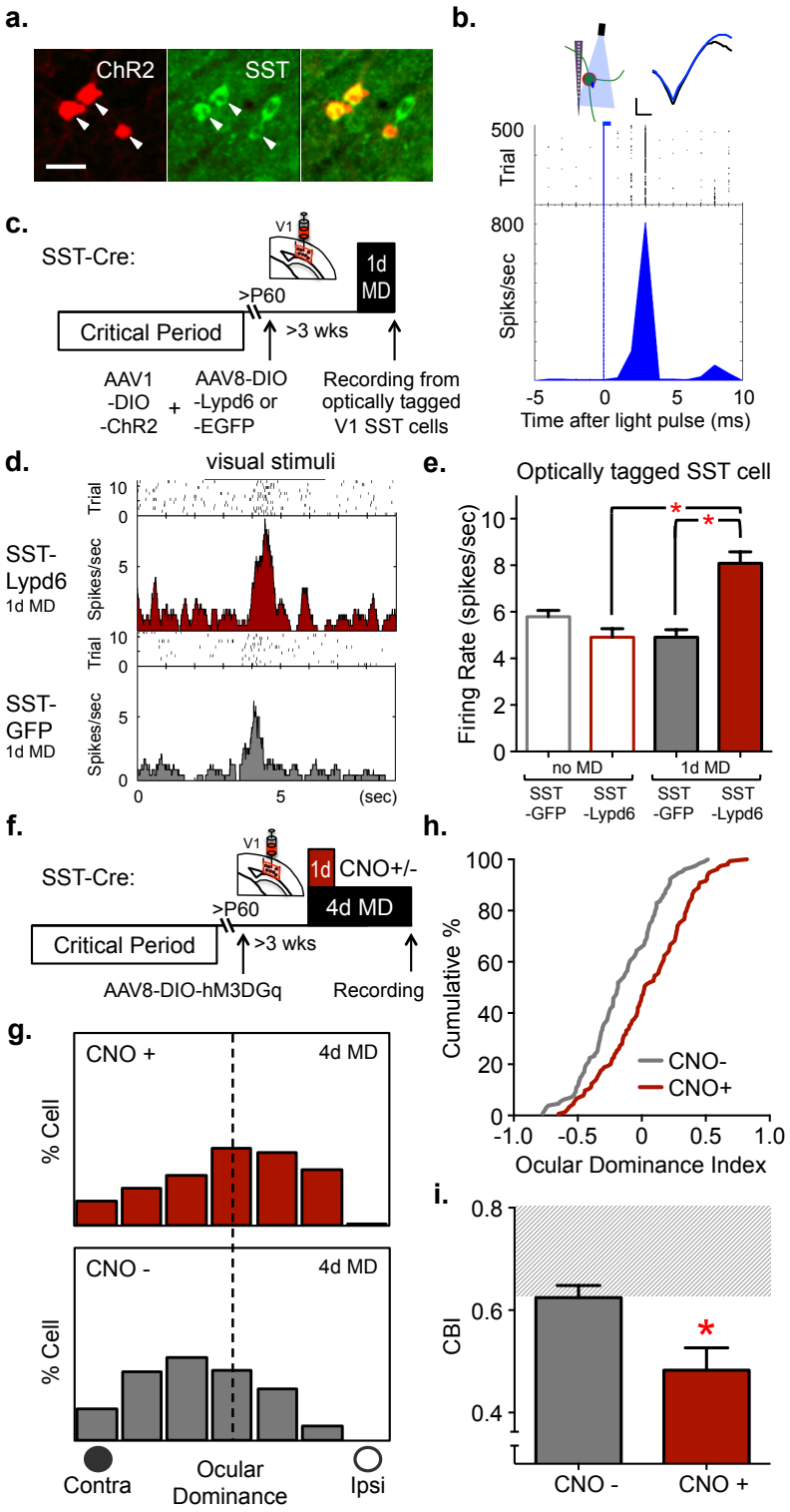

Figure 4 | Lypd6 in SST interneurons increase SST interneuron activity to express ocular dominance plasticity. (a) Representative images of viral mCherry labeling following injection of AAV-

ChR2 into the V1 of SST-cre mice. ChR2/mCherry (red) is specifically expressed in immunolabeled SST (green) neuron. 95±1.86% of mCherry labeled cells co-labeled with SST. [n=2 mice]. Data is mean±SEM. Scale bar=25μm. **(b)** Example of an optically-tagged SST interneuron showing time locked optogenetic activation. Laser (wavelength 473 nm, fiber diameter 105 μm) was delivered using an optic fiber coupled to the multichannel extracellular recording electrode. The fiber tip was positioned immediately above the V1 recording site. SST+ cells were identified with a light pulse (1ms, 20Hz) stimulus. **(c)** Schematic representation of experiment for **d-e**. Adult (>P60) SST-cre mice were injected with a combination of AAV-ChR2 and either AAV-Lypd6 (SST-Lypd6) or AAV-EGFP (SST-GFP) into V1 binocular zone and incubated for >3 weeks prior to 1 day of monocular deprivation (1d MD), after which extracellular recordings were conducted to collect and analyze visually evoked firing rates of optically-tagged SST interneurons. **(d)** Representative histograms of visually evoked firing of optically-tagged SST interneurons after adult 1d MD in SST-Lypd6 [top, red] and SST-GFP [gray, bottom]. **(e)** Comparison of visually evoked firing rate following adult 1d MD in SST-GFP [gray solid bar; n=68 cells, 4 mice] and SST-Lypd6 [red solid bar; n=101 cells, 5 mice] with non-deprived (no MD) SST-GFP [gray open bar; n=82 cells, 5 mice] and SST-Lypd6 [red open bar; n=38 cells, 3 mice]. Data in figure presented as cell-level mean±SEM. Overexpression of Lypd6 results in a significant increase in visually evoked firing rate of SST interneurons after 1d MD (SST-Lypd6 1d MD) in comparison to SST-GFP 1d MD and SST-Lypd6 no MD (respectively, $*P=0.0137$ and $*P=0.0339$, *Linear Mixed Model (LMM)* – animal considered as random effect, genetic manipulation (-GFP or -Lypd6) and experience (1d MD or no MD) considered as fixed effects; multiple comparisons corrected by Tukey's method). **(f)** Schematic representation of V1 plasticity paradigm by 4d MD with viral injection. AAV-GqDREADD was injected into V1 binocular zone of adult SST-cre mice and incubated for >3 weeks prior to 4d MD. CNO (CNO+) or saline (CNO-) was given during the first day of 4d MD to chemogenetically activate viral GqDREADD expressing SST interneurons for only 1 day. Following 4d MD, extracellular recordings were performed for analysis of ocular dominance. **(g)** Chemogenetic activation of SST interneurons during the first day of 4d MD through CNO delivery [CNO+: red, n=154 cells from 5 mice] results in a significant shift in

ocular dominance distribution, but not when given saline [CNO-: gray, n=129 cells from 5 mice]: ***P=0.0007, χ^2 test. **(h)** Cumulative plot of ocular dominance index after adult 4d MD confirms ocular dominance shift after 1 day-activation of SST interneurons in CNO+ mice [red line, n=154 cells from 5 mice] compared with CNO- [gray line, n=129 cells from 5 mice]: **P<0.0001, K-S test. **(i)** Comparison of contralateral bias index (CBI) following 4d MD in SST-cre mice injected with AAV-GqDREADD and administered either CNO [CNO+: red solid bar, CBI=0.50; n=5 mice] or saline [CNO-: gray solid bar, CBI=0.62; n=5 mice] during the first day of 4d MD: *P=0.0208, Student's t-test. Gray background area represents CBI range in a non-plastic mouse. Data in figure presented as mean±SEM.

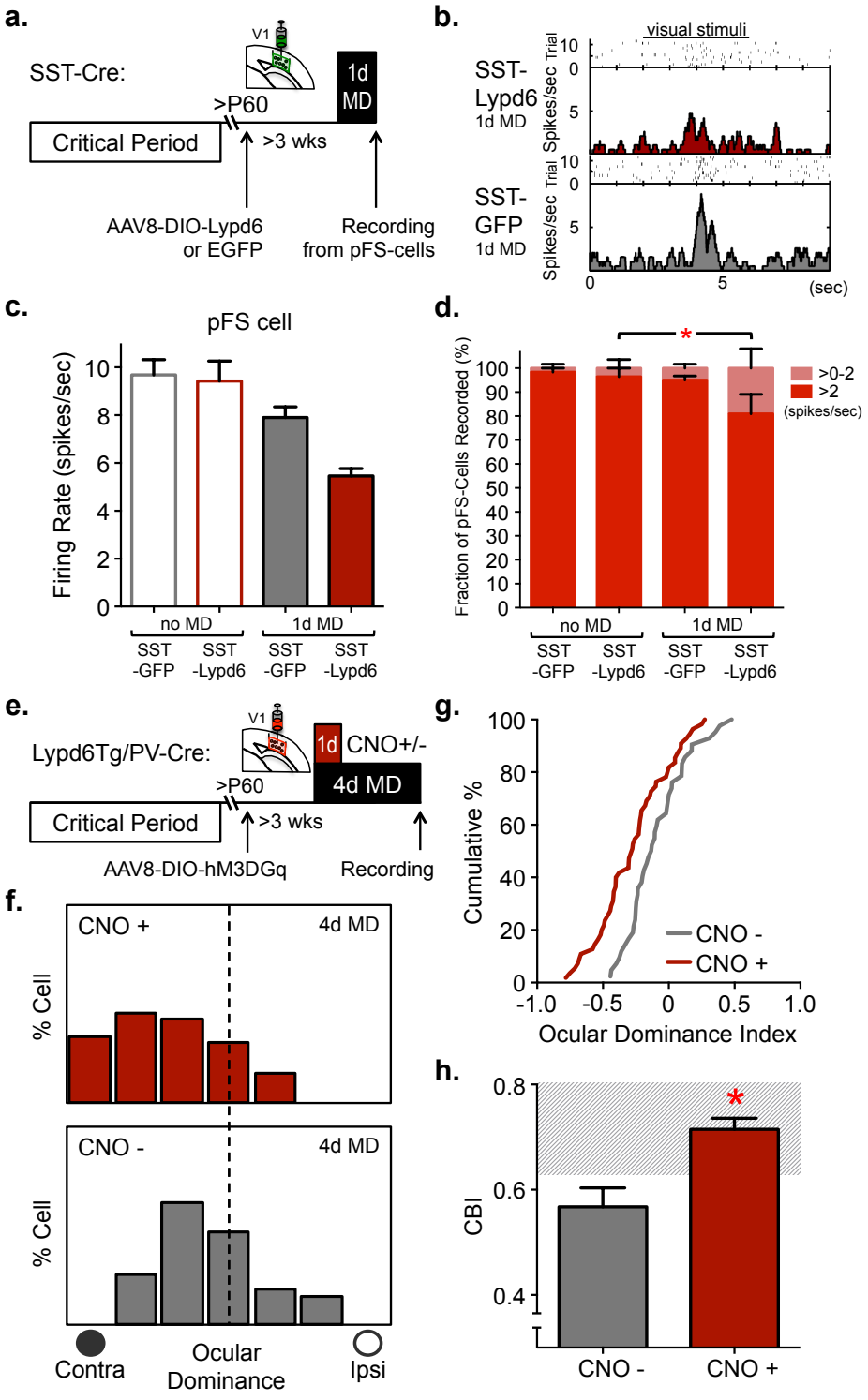

Figure 5 | Lypd6 in SST interneurons suppress PV interneuron activity to express ocular dominance plasticity. (a) Schematic representation of experiments in **b-c**. Adult (>P60) SST-cre mice were injected with AAV-Lypd6 (SST-Lypd6) or AAV-EGFP (SST-GFP) into V1 binocular zone and

incubated for >3 weeks prior to 1d MD, after which extracellular recordings were conducted to collect and analyze visually evoked firing rates of putative fast-spiking (pFS) cells sorted by their narrow spike width. For sorting details see *Methods* and Supplementary Figure 4. **(b)** Representative histograms of visually evoked firing of pFS cells after adult 1d MD in SST-Lypd6 [top, red] and SST-GFP [gray, bottom]. **(c)** Comparison of cell-level means of visually evoked firing rate show a trending reduction with no statistical significance in visually evoked firing rate of pFS cells in SST-Lypd6 1d MD [red solid bar; n=170 cells, 7 mice], in comparison to all other groups when fitted to a *Linear Mixed Model (LMM)*: SST-GFP 1d MD [gray solid bar; n=148 cells, 5 mice], SST-Lypd6 no MD [red open bar; n=63 cells, 4 mice], and SST-GFP no MD [gray open bar; n=116 cells, 5 mice] confirmed by pairwise tests with SST-GFP 1d MD, SST-Lypd6 no MD, and SST-GFP no MD (respectively, P=0.211, P=0.2301, and P=0.1161 – animal considered as random effect, genetic manipulation (-GFP or -Lypd6) and experience (1d MD or no MD) considered as fixed effects; multiple comparisons corrected by Tukey's method). All other comparisons under LMM between SST-Lypd6 no MD, SST-GFP no MD, and SST-GFP 1d MD have P>0.98. Data in figure presented as cell-level mean±SEM. **(d)** Adult SST-Lypd6 1d MD shows significant reduction of the fraction of pFS neurons with higher firing frequency (Bin/separation: neurons with >2 spikes/sec): *P=0.0259, one-way ANOVA; SST-Lypd6 1d MD [n=7 mice, 170 cells] vs. SST-Lypd6 no MD [n=4 mice, 63 cells]: diff=-0.18, *P= 0.036, vs. SST-GFP no MD [n=5 mice, 116 cells]: diff=-0.16, ^{t}P=0.06, Tukey's multiple comparisons test). Data in figure presented as mean±SEM. **(e)** Schematic representation of V1 plasticity paradigm by 4d MD with viral injection. AAV-GqDREADD was injected into V1 binocular zone of adult bigenic Lypd6Tg/PV-cre mice and incubated for >3 weeks prior to 4d MD. CNO (CNO+) or saline (CNO-) was given during the first day of 4d MD to chemogenetically activate viral GqDREADD expressing PV interneurons for only 1 day. Following 4d MD, extracellular recordings were performed for analysis of ocular dominance. **(f)** Chemogenetic activation of PV interneurons during the first day of 4d MD through CNO delivery [CNO+: red, n=55 cells from 4 mice] results in a significant decrease in ocular dominance shift, but not when given saline [CNO-: gray, n=42 cells from 3 mice]: **P=0.0030, χ^2 test. **(g)** Cumulative plot of

ocular dominance index after adult 4d MD confirms decreased ocular dominance shift after 1 day-activation of PV interneurons in CNO+ mice [red line, n=55 cells from 4 mice] compared with CNO- [gray line, n=42 cells from 3 mice]: ***P*=0.0054, K-S test. **(h)** Comparison of contralateral bias index (CBI) following 4d MD in SST-cre mice injected with AAV-GqDREADD and administered either CNO [CNO+: red solid bar, CBI=0.71; n=4 mice] or saline [CNO-: gray solid bar, CBI=0.57; n=3 mice] during the first day of 4d MD: **P*=0.0128, Student's *t*-test. Gray background area represents CBI range in a non-plastic mouse. Data in figure presented as mean±SEM.